EcoMat
Open Access
FUNCTIONAL MATERIALS FOR GREEN ENERGY AND ENVIRONMENT

WILEY

Passive Daytime Radiative Cooling: Fundamentals, Material Designs, and Applications

Meijie Chen*, Dan Pang, Xingyu Chen, Hongjie Yan, Yuan Yang*

Prof. M. Chen, D. Pang, X. Chen, Prof. H. Yan
School of Energy Science and Engineering, Central South University, Changsha 410083, China
E-mail: chenmeijie@csu.edu.cn (M. Chen)

Prof. Y. Yang
Department of Applied Physics and Applied Mathematics, Columbia University, New York 10027, United States
E-mail: yy2664@columbia.edu (Y. Yang)

Keywords: radiative cooling; solar reflectance; thermal emittance; coating; daytime

Abstract: Passive daytime radiative cooling (PDRC) dissipates terrestrial heat to the extremely cold outer space without using any energy input or producing pollution. It has the potential to simultaneously alleviate the two major problems of energy crisis and global warming. In this review, we summarize general strategies implemented for achieving PDRC and various applications of PDRC technologies. We first introduce heat transfer processes involved in PDRC, including radiative and nonradiative heat transfer processes, to evaluate the PDRC performance. Subsequently, we summarize the general material designs used for controlling PDRC performance, such as tuning the thermal mid-infrared emittance and solar reflectance. Finally, we discuss the diverse applications of PDRC technologies to overcome problems in space cooling, solar cell cooling, water harvesting, and electricity generation.

1. Introduction

Over the years, cooling has become more critical to human life because of global warming, population growth, and industrial development. However, the current compression-based cooling systems consume a lot of electricity and produce large amounts of CO_2. Moreover, the typical refrigerants applied in these systems destroy the ozone layer.[1] In addition, traditional cooling systems only transfer heat to different places on Earth, which increases environmental temperature and cooling load power.[2] Therefore, with increasing awareness about the energy crisis and environmental problems, improving the cooling efficiency of existing systems and finding new alternatives are becoming crucial. [3]

Radiative cooling systems can realize passive cooling, which transfers excess heat to outer space through thermal radiation based on the large temperature difference between the Earth (~ 300 K) and outer space (~ 3 K), [4-7]. These systems emit infrared thermal radiation from the Earth's surface through the atmosphere to outer space to achieve cooling without any energy consumption. For the past several centuries, radiative cooling has been used for terrestrial entity cooling and water harvesting during nighttime in tropical and subtropical regions.

More than 2000 years ago, ancient Iranians and Indians employed radiative cooling to produce and store ice in ice-making basins or ice pits, although the ambient temperature was above the freezing point.[8] In 1828, Arago first reported this phenomenon and found that the temperatures of grass, cotton, and quilt placed outdoors at night were 6–8 K lower than the ambient temperature.[9] In 1959, Head first used a selective infrared emitter to improve nighttime radiative cooling performance. Nighttime radiative cooling has been extensively studied over the past few decades.[10] However, passive daytime radiative cooling (PDRC) has higher requirements on materials and structures to avoid solar heating.

With the development of radiative cooling technologies in recent years, PDRC can be achieved by reflecting solar radiation and increasing thermal mid-infrared emittance.[11,12] The PDRC coating needs a high solar reflectance ($\bar{R}_{\mathrm{solar}}$) in the solar spectrum (0.3–2.5 μm) to

avoid solar heating, and a strong thermal emittance ($\bar{\varepsilon}_{\mathrm{LWIR}}$) in the atmospheric long-wave infrared (LWIR) transmission window (8–13 μm) to lose energy to the cold sky. Hence, even during daytime, the heat loss to the cold outer space by thermal radiation through the atmospheric LWIR window is significantly larger than the heating from sunlight, thereby achieving electricity-free spontaneous cooling.[13,14]

Recently, various PDRC coatings with high $\bar{R}_{\mathrm{solar}}$ and $\bar{\varepsilon}_{\mathrm{LWIR}}$, such as photonic structures,[4] polymers,[15] dielectrics,[16,17], and dielectric-polymer composites,[18] have been developed. The intrinsic absorptance of polymers and dielectric materials can usually provide a high emittance in the atmospheric LWIR window. Thus, achieving a near-perfect solar reflectance is significant for achieving PDRC. In the past decade, various materials or structures have been proposed to reflect solar radiation and achieve high cooling performance, including covering a bulk polymer on a metal solar reflector (such as Ag and Al),[11,19] and using porous or microspherical structures where the curved interface (such as the SiO_2-air, air-polymer, and SiO_2-polymer interfaces) amplifies solar scattering.[20-23] Some previous reviews have been conducted to summarize existing material designs to achieve PDRC from the whole spectrum.[13,24-27] While little attention is paid to the sub-band spectrum design from the solar spectrum (including colored coatings) and LWIR spectrum (selective or angle-dependent coatings), and their dynamic switchable spectrum based on the solar spectrum or LWIR spectrum.

Therefore, in this review, we first introduce the fundamentals of PDRC, followed by summarizing the material and structural designs to improve thermal LWIR emittance (including the broadband, selective, or angle-dependent emittance) and solar reflectance (including colored coatings), and the dynamic switchable regulations of cooling coatings from the solar spectrum or LWIR spectrum. Finally, we discuss various applications of PDRC, such as space cooling, solar cell cooling, water harvesting, and electricity generation.

2. Fundamentals of PDRC coatings

According to Kirchhoff's law, materials with a temperature above 0 K continuously absorb and emit electromagnetic waves. Heat is exchanged among objects at different temperatures by absorbing and emitting these electromagnetic waves.[24] Earth has been experiencing this phenomenon by radiating heat to the cold outer space. Therefore, the temperature of Earth gradually decreases at night because its temperature (~ 300 K) is much higher than that of outer space (~ 3 K) and there is no solar heating at night. [12] When the heat absorbed by the coating is less than the energy radiated to the cold outer space, the coating achieves electricity-free cooling even during the daytime (Figure 1a), which is the basic principle of PDRC.[28]

2.1. Solar reflectance and thermal LWIR emittance of PDRC coatings

PDRC requires precise control of the optical performance of the coating over a wide spectrum (from UV to mid-infrared). Figure 1b shows the ideal spectrum of a PDRC coating: (a) In the solar spectrum (0.3–2.5 μm), the absorptance should be 0 (100% reflectance) to avoid solar heating. (b) In the atmospheric LWIR transmission window (8–13 μm), the emittance should be 1 to effectively radiate heat to outer space through this partially transparent atmosphere window. (c) In other mid-infrared wavelengths (2.5–8 μm and >13 μm), the emittance should be 0 to avoid the overheating of the atmospheric irradiation at a higher temperature than that of the PDRC coating. The temperature difference between the atmosphere and PDRC coating is small (5–10 °C) in most cases; however, this can be ignored when compared with the first two effects. [2,8,12] Thus, the solar reflectance ($\bar{R}_{\mathrm{solar}}$) and thermal LWIR emittance ($\bar{\varepsilon}_{\mathrm{LWIR}}$) are typically considered in the PDRC design.

$\bar{R}_{\mathrm{solar}}$ is the ratio of the reflected solar intensity to the integral solar intensity in λ = 0.3–2.5 μm, which can be expressed as follows:

$$\bar{R}_{\mathrm{solar}} = \frac{\int_{0.3\mu\mathrm{m}}^{2.5\mu\mathrm{m}} I_{\mathrm{solar}}(\lambda) R(\lambda) \mathrm{d}\lambda}{\int_{0.3\mu\mathrm{m}}^{2.5\mu\mathrm{m}} I_{\mathrm{solar}}(\lambda) \mathrm{d}\lambda}, \quad (1)$$

where $I_{\mathrm{solar}}(\lambda)$ represents the ASTM G173-03 global solar intensity spectrum at AM 1.5 and $R(\lambda)$ is the spectral reflectance of the coating.

Similarly, $\bar{\varepsilon}_{\mathrm{LWIR}}$ is expressed as follows:

$$\bar{\varepsilon}_{\mathrm{LWIR}} = \frac{\int_{8\mu m}^{13\mu m} I_{\mathrm{bb}}(T,\lambda)\varepsilon(T,\lambda)\mathrm{d}\lambda}{\int_{8\mu m}^{13\mu m} I_{\mathrm{bb}}(T,\lambda)\mathrm{d}\lambda}, \quad (2)$$

where $I_{\mathrm{bb}}(T,\lambda)$ is the spectral intensity emitted by a standard blackbody with temperature T and $\varepsilon(T,\lambda)$ represents the spectral emittance of the sample.

2.2. Cooling power of PDRC coatings

In the daytime, the net cooling power of a PDRC coating is a combination of solar radiation, coating, atmospheric thermal radiation, and nonradiative heat transfer (Figure 1a), and can be expressed as follows:

$$P_{\mathrm{net}} = P_{\mathrm{rad}} - P_{\mathrm{atm}} - P_{\mathrm{solar}} - P_{\mathrm{nonrad}}, \quad (3)$$

where P_{net} is the net cooling power. P_{rad} is the radiative power of the coating. P_{atm} and P_{solar} are the absorbed powers from the atmospheric and solar irradiations, respectively. P_{nonrad} is the total power loss of all nonradiative heat transfer processes, such as convective and thermal conduction between the coating and the ambient environment.

2.2.1. Radiative power of PDRC coatings

The radiative power (P_{rad}) of a PDRC coating is a function of the coating temperature T_{c} and the emittance spectrum of the PDRC, which can be expressed as follows:

$$P_{\mathrm{rad}}(T_{\mathrm{c}}) = \int \cos\theta \, \mathrm{d}\Omega \int_0^{\infty} I_{\mathrm{bb}}(\lambda, T_{\mathrm{c}})\varepsilon(\Omega,\lambda)\, \mathrm{d}\lambda, \quad (4)$$

where $\int \mathrm{d}\Omega = \int_0^{\pi/2} \sin\theta \, \mathrm{d}\theta \, \mathrm{d}\varphi$ is the angular integral on a hemisphere, I_{bb} is the spectral radiation power of the blackbody, T_{c} is the PDRC coating temperature, and ε is the coating emittance.

For PDRC applications, P_{rad} is absorbed by the atmosphere and outer space, which can be assumed to be a blackbody system $\varepsilon = 1$. While the temperature of outer space is as low as 3 K, the radiation power of outer space can be ignored. Furthermore, the radiation power of the atmosphere should be considered because its temperature is similar to that of the coating, which will be discussed in the next section. In the range of T_{c} = 0–50 °C, the radiation peak of the

blackbody is located in the atmospheric LWIR window, and more radiation can be emitted to outer space (Figure 2a).[30] Therefore, a near-perfect emittance spectrum ($\varepsilon = 1$) at λ = 8–13 μm is usually required to improve the PDRC performance. Furthermore, higher radiation power based on an ideal emitter (Figure 1b) can be achieved at a higher T_c (Figure 2b) because of the fourth-power relationship between the radiation power and temperature.

For most PDRC experiments with open and unobstructed surroundings, the emittance is nearly angle-independent over a wide angular range (0–80°) [31-30], and the change of emittance in the experimental temperature range is small. Thus, ε is usually assumed to be independent of temperature and angle. However, it is important to consider direction-dependent emittance when the coating is not fully horizontal or the surrounding environment is not open and unobstructed because radiation from the ground cannot be ignored.

2.2.2. Absorbed power from atmospheric irradiation

The absorbed power from atmospheric irradiation (P_{atm}) is related to the coating emittance ε (absorptance), atmospheric emittance $\varepsilon_{\mathrm{atm}}$, and temperature T_{amb}, which can be expressed as follows:

$$P_{\mathrm{atm}}(T_{\mathrm{amb}}) = \int \cos\theta \, d\Omega \int_0^{\infty} I_{\mathrm{bb}}(\lambda, T_{\mathrm{amb}}) \varepsilon(\Omega, \lambda) \varepsilon_{\mathrm{atm}}(\Omega, \lambda) \, d\lambda, \quad (5)$$

where $\int d\Omega = \int_0^{\pi/2} \sin\theta \, d\theta \, d\varphi$ is the angular integral on a hemisphere; $I_{\mathrm{bb}}(\lambda, T)$ is the spectral radiation of a blackbody at temperature T; and $\varepsilon_{\mathrm{atm}}(\theta, \lambda)$ is the atmospheric emittance as a function of direction and wavelength, which can be obtained by $\varepsilon_{\mathrm{atm}}(\theta, \lambda) = 1 - t(\lambda)^{1/\cos\theta}$, where $t(\lambda)$ is the atmospheric transmittance in the zenith direction.

Figure 3a shows the atmospheric transmittance in the mid-infrared region. A large transmittance or small emittance can be achieved at λ = 8–13 μm, which is also called the first atmospheric transparent window. In this region, the atmosphere is highly transparent, and most thermal radiation can be emitted into outer space.[32] The atmospheric transmittance depends on the zenith angle, cloud cover latitude, and air humidity. For example, considering the effect of

air humidity, the atmospheric transmittance decreases with an increase in the water column because of the infrared absorptance of water vapor (Figure 3a), which would reduce the radiative cooling power (Figure 3b).[34]

To clarify the interrelationship between $P_{\mathrm{rad}}(T_{\mathrm{c}})$ and $P_{\mathrm{atm}}(T_{\mathrm{amb}})$, it can be seen that when $T_{\mathrm{c}} = T_{\mathrm{amb}}$, $P_{\mathrm{atm}}(T_{\mathrm{amb}})$ is almost equal to the absorbed power of the atmosphere from the coating irradiation and the cooling power is equal to the radiative power emitted into outer space through the atmospheric LWIR window, which can be expressed as follows:

$$P_{\mathrm{rad}}(T_{\mathrm{c}}) - P_{\mathrm{atm}}(T_{\mathrm{amb}}) = \int \cos\theta \, d\Omega \int_0^{\infty} I_{\mathrm{bb}}(\lambda, T)\varepsilon(\Omega, \lambda)[1 - \varepsilon_{\mathrm{atm}}(\Omega, \lambda)] \, d\lambda \quad (6)$$

The value of $P_{\mathrm{rad}}(T_{\mathrm{c}}) - P_{\mathrm{atm}}(T_{\mathrm{amb}})$ is mainly determined by the radiative power at λ = 8–13 μm because of the first atmospheric LWIR window. Therefore, $\bar{\varepsilon}_{\mathrm{LWIR}}$ in Equation (2) is usually used to determine the thermal radiation behavior of PDRCs in the mid-infrared region, as shown in Figure 3c.

When $T_{\mathrm{c}} < T_{\mathrm{amb}}$, $P_{\mathrm{atm}}(T_{\mathrm{amb}})$ is larger than the absorbed power of the atmosphere from the coating irradiation; this would heat the coating because of the infrared absorption from atmosphere irradiation out of the range λ = 8–13 μm. Moreover, when $T_{\mathrm{c}} > T_{\mathrm{amb}}$, the PDRC performance would improve because of the lower infrared absorption from the atmosphere irradiation out of the range λ = 8–13 μm. Therefore, to standardize the calculation of cooling power, $T_{\mathrm{c}} = T_{\mathrm{amb}}$ is generally used to calculate the net cooling power, where a higher coating temperature T_{c} improves the cooling power. Simultaneously, the secondary atmospheric window (16–28 μm) may provide an additional maximal cooling power of 20 W m^{-2},[35] which is usually ignored because of its weak transmittance, especially at high air humidity, as shown in Figure 3a.

2.2.3. Absorbed power from solar irradiation

Sunlight is attenuated after traveling through the atmosphere because of the scattering and absorption of atmospheric components. Figure 4a shows the solar spectral irradiance of the

extraterrestrial (AM 0), global tilted, and direct normal spectra at AM 1.5, where it can be observed that the solar irradiation is mainly concentrated at λ = 0.3–2.5 μm. The global solar irradiation flux can reach 1000 W m^{-2} for a clear sky, with the diffuse component typically in the range of 50–100 W m^{-2}.[9] The formula for calculating the solar irradiation absorbed by the PDRC can be expressed as follows:

$$P_{\text{solar}} = \int_{0.3\text{um}}^{2.5\text{um}} \varepsilon(\theta, \lambda) I_{\text{solar}}(\lambda)\, d\lambda, \tag{7}$$

where θ is the incident angle of solar irradiation. $\varepsilon(\theta, \lambda)$ is the coating emittance as a function of direction and wavelength. $I_{\text{solar}}(\lambda)$ is the direct spectral solar irradiation.

For PDRC under sunlight, the effect of solar heating on PDRC performance is significant. The typical cooling power of a high-performance PDRC coating is approximately 100–150 Wm^{-2} at T = 25 °C, while the global solar radiation can be as high as 1000 W m^{-2}. The solar reflectance of PDRC coatings should be larger than 0.9 to achieve cooling performance in the daytime. Therefore, in practical PDRC applications, $\bar{R}_{\text{solar}}$ should be > 0.95, or at least > 0.9, and $\bar{\varepsilon}_{\text{LWIR}}$ should be over 0.7, preferably above 0.9.

2.2.4. Nonradiative heat transfer

Nonradiative heat transfer (convection and conduction) should be considered to evaluate the performance of PDRC. The nonradiative loss can be expressed as follows:

$$P_{\text{nonrad}} = h(T_{\text{amb}} - T_{\text{c}}), \tag{8}$$

where h is the total heat transfer coefficient, which accounts for the convection and conduction heat transfer between the environment and PDRC coating.

The conduction heat transfer is mainly determined by the surrounding materials of the PDRC coating, whereas the convection heat transfer depends on the wind speed over the PDRC coating.[8,12,36] In PDRC experiments, several devices are proposed to minimize the effect of nonradiative heat transfer (Figure 5) and to evaluate the PDRC performance. A direct solution is to place the PDRC coating on a substrate directly exposed to the ambient atmosphere, as

shown in Figure 5a, thereby resulting in $T_c < T_{amb}$. In this device, a thermal insulation substrate is used to avoid conduction heat transfer between the coating and the substrate. However, convection heat transfer between the air and coating, which would heat the coating because $T_c < T_{amb}$, cannot be ignored. To avoid convection heat transfer, a convection shield can be employed at the top to suppress thermal losses, as shown in Figure 5b, and the temperature difference between the radiative cooling surface and ambient temperatures ($T_c - T_{amb}$) can be used to characterize the PDRC performance. To measure the net cooling power, a heater with controlled power can be placed under the PDRC coating to maintain $T_c = T_{amb}$ and the heating power is equal to the net cooling power, as shown in Figure 5c.

As discussed above, the cooling power of PDRC coatings can be measured at $T_c = T_{amb}$ while the temperature decrease is obtained at $T_c < T_{amb}$, which are determined by the thermal boundary (temperature, convection, and conduction) and atmospheric conditions. Table 1 lists the PDRC performance of some reported works. It can be found that the cooling power is about 40–130 W m^{-2} at the ambient temperature of 300–310 K while the temperature decrease is 2–15 K. It's difficult to compare the PDRC performance by the cooling power and temperature decrease since the experiment setup and atmospheric condition are various in different works. Hence, in the following section, we will focus on the fundamental spectral design to achieve PDRC.

Table 1 List of types, materials, thickness, solar reflectance, thermal LWIR emittance, temperature decrease, and cooling power of the previously reported PDRC coatings

Author & Year	Structure & Material	Thickness	Solar reflectance	Thermal emittance	Cooling power W/m^2	Temperature decrease	Solar intensity W/m^2	Ambient temperature	Remark
E. Rephaeli [11] in 2013	Quartz-SiC-MgF_2-TiO_2-Ag	1.8 μm	0.965	/	105	/	964	300 K	Sim.
A.P. Raman [4] in 2014	HfO_2-SiO_2-Ag	1.6 μm	0.97	/	40.1	4.9 °C	850	/	Exp.
Z. Chen [19] in 2016	Si_3N_4-Si-Al	0.92 μm	/	/	/	4.2 °C	/	/	Exp.
J. long Kou [37] in 2017	PDMS-SiO_2-Ag	720 μm	/	/	127	8.2 °C	/	300 K	Exp.
Z Huang [23] in 2017	Acrylic resin-TiO_2	500 μm	0.9	>0.9	100	/	900	300 K	Sim.
J. Mandal [15] in 2018	Porous PVDF	~300 μm	0.96±0.03	0.97±0.02	96	6 °C	890	/	Exp.
S. Gamage [38] in 2019	Porous cellulose	275 μm	>0.9	~0.9	/	15 °C	/	/	Exp.
A. Lerory [39] in 2019	Porous PEA	6 mm	0.922	0.799	96	13 °C	936	298K	Exp.
J. Fernandez [40] in 2019	SiO_2 spheres	8 μm	0.97	>0.9	107-125	/	800	/	Exp.
L.Zhou [32] in 2019	PDMS-Al	150 μm	/	/	120	~2-9 °C	~853.5	/	Exp.
E.Lee [41] in 2019	PDMS-Ag	220 μm	/	/	/	11 °C	1000	300K	Sim.
T. Suichi [42] in 2020	PMMA+SiO_2-PDMS-Ag	27 μm	/	/	/	2.3 °C	778	>309.5K	Exp.
J. Song [30] in 2020	PDMS-Ag	>100 μm	/	0.99	/	/	/	/	Exp.
E. Blandre [43]	SiO_2-Ag	>500 μm	/	/	114	/	/	300 K	Sim.

in 2020									
H. Zhang [44] in 2020	PDMS+Al_2O_3 spheres	500 μm	~0.95	>0.96	~90.8	5.1 °C	862	305 K	Exp.
X. Li [45] in 2020	Acrylic + $CaCO_3$ particles	~400 μm	0.955	0.94	37	1.7 °C	963	/	Exp.
W. Fuqiang [46] in 2020	TiO_2 + SiO_2 spheres	/	0.956	0.949	/	/	/	/	Sim.
X. Wang.[47] in 2020	Porous PVDF + SiO_2 spheres	300 μm	0.97	0.96	61	6 °C	1000	305K	Sim.
A. Zining [48] in 2020	acrylic resin +SiO_2 spheres	70 μm	/	0.937	108.49	8.7 °C	952	/	Exp.
R. Yalcln [49] in 2020	PDMS+SiO_2 +Ag	500 μm	/	/	114	/	/	300K	Sim.
H. Zhao [50] in 2020	Porous PDMS	500 μm	0.93	0.94	/	5 °C	950	308K	Exp.
D. Chae [51] in 2020	SiO_2-Si_3N_4-Al_2O_3-Ag	502 μm	0.948	0.87	/	8.3 °C	872	/	Exp.
X. Nie [52] in 2020	PDMS + glass bubbles	750 μm	0.92	0.85	78	5.3 °C	780	/	Exp.
F. Wang [53] in 2021	PMMA + Si_3N_4 + Al_2O_3 particles	35 μm	0.915	0.9958	/	/	/	/	Sim.
S. Zhong [54] in 2021	Cotton + PDMS-$AlPO_4$	/	0.97	0.94	/	5.4 °C	998	310 K	Exp.
B. Xiang [55] in 2021	Porous PCA + SiO_2 spheres	150 μm	0.96	0.95	/	6.2 °C	900	/	Exp.
K. Zhou [56] in 2021	Porous PE + SiO_2 spheres	840 μm	0.962	>0.9	85	6.1 °C	747	/	Exp.
J. Zhang [57] in 2021	Polyester fabrics	200 μm	0.95	/	48	4.9 °C	/	/	Exp.
C. Feng [58] in 2021	PVDF + Li-PAAm hydrogel	2 mm	/	/	150*	7 °C	800	/	Exp.
M. Chen [59]	PVDF-Al	300 μm	0.98	0.984	72	/	/	298K	Sim.

in 2021									
D. Chae [60] in 2021	acrylate + Al_2O_3 + SiO_2 particles	/	0.941	0.935	100	7.9 °C	/	300K	Exp.
Y. Zhu [61] in 2021	SiO_2- Si_3N_4-Al_2O_3-Ag	~ 1.43 μm	0.966	0.908	84.1	8.6 °C	/	300K	Sim.

* This cooling power includes evaporative cooling and radiative cooling.

3. Material Designs for PDRC

To achieve effective PDRC, a structure should not only achieve a solar reflectance much higher than 0.9 but should also exhibit a high emittance value (> 0.9) in the atmospheric LWIR transparent window. In this section, we summarize the materials and structure design for solar reflectance and thermal mid-infrared emittance.

3.1. Thermal mid-infrared emittance

To achieve better PDRC performance in sub-ambient conditions, diverse materials have been proposed to improve the mid-infrared emittance where λ = 8–13 μm. These structures can be categorized into inorganic dielectric materials and organic polymer materials,[15,62-65] as shown in Figure 6. Both types of materials are almost transparent (k is almost 0) in the solar spectrum to avoid solar absorption or heating, and exhibit strong absorption (k is large) in the atmospheric LWIR window, and emit more heat to the deep outer space.[65,66]

3.1.1. Improved thermal mid-infrared emittance

Inorganic dielectric materials can achieve spectrally selective infrared emittance because of the wide absorption band of metal-O bonds.[40,51] In addition, Al_2O_3, TiO_2, and SiO_2 are stable and chemically inert materials, and inorganic coatings inherently exhibit superior mechanical robustness and retainability, thereby guaranteeing a long lifespan in exterior environments. Thus, a simple bulk dielectric multilayer can achieve a selective thermal mid-infrared emittance spectrum(Figure 7a).[4,51,61] In addition, high-performance PDRC performance can be obtained by more complex photonic multi-layer structures to increase the emittance in the LWIR atmospheric window.[11] However, these multi-layer dielectric layers or structures usually have submicron level dimensions (Figure 7a), and their fabrication requires complex processing methods, such as etching and magnetron sputtering.

Compared with bulk dielectric films, dielectric microsphere coatings can be easily prepared by painting, and a high emittance can be achieved by tuning the fill rate and sphere radius because of the dipole resonance of microspheres in the mid-infrared region (Figure

7b).[20,40,67] However, these dielectric microsphere coatings have various problems, such as lack of flexibility, water-repellence, and anti-abrasion. Furthermore, by incorporating dielectric microspheres in a polymer, a flexible and water-repellent PDRC coating can be obtained, and the LWIR emittance can be further improved (> 0.95) and adjusted by the polymer, volume fraction, and radius of the microspheres (Figure 7c).[18,23]

Recently, polymer-based PDRC coatings and paints have gained considerable attention because of their potential for large-scale production, low cost, and applicability to various systems. The infrared "fingerprint" of polymers with many functional groups/bonds, such as C-F and C-O, overlap with the atmospheric LWIR transmittance window and are responsible for the high thermal mid-infrared emittance of polymers.[33,65] Thus, nonporous polymer coatings, such as PDMS, PMMA, and PVDF with a thickness of ~200 μm, usually have an average LWIR emittance of 0.95 (Figure 8a) because of the intrinsic absorption ability of polymers.[33,68] To reduce material consumption, the emittance in the atmospheric LWIR window can be improved significantly at a thickness of 28.5 μm by the broadband localized surface plasmon resonance of self-doped In_2O_3 nanoparticles (4.5%) (Figure 8b). However, these polymer coatings could not achieve near-perfect emittance in the atmospheric LWIR window by increasing the polymer thickness because of the inevitable interface reflection between the air and polymer, and the maximal $\bar{\varepsilon}_{LWIR}$ = 0.95 at 25 °C.

A near-perfect emittance $\bar{\varepsilon}_{LWIR}$ = 0.99, which can be achieved by modifying the coating surfaces with some microstructures (such as grating patterns,[30,68] and wrinkles [53]) to reduce the interface reflectance in the mid-infrared region (Figure 8c). These surface microstructures require expensive templates during the preparation process, thereby limiting large-scale applications.[44] Similarly, by coupling the effect of microspheres and microstructure surfaces (Figure 8d), polymer coatings with a porous surface can potentially be used for PDRC application; these coatings can be easily painted by the volatilization of the solvent,[15] or the dissolution of the sphere template.[31,69] A high value of $\bar{\varepsilon}_{LWIR}$ = 0.97 at 25 °C has been achieved

in both experiments and simulations.[15,59] However, the volatile solvent used in the preparation of porous coatings increases the content of volatile organic compounds (VOCs). To overcome this issue, an aqueous processing-based polymer coating with both excellent PDRC performance and low VOC content was reported by the assembly of nanoparticles into uniform micro-clusters. [70]

In addition, the fabric structure can also achieve PDRC, which incorporates PDRC into personal thermal management technologies. Much work has been done for mid-infrared (MIR)–transparent radiative cooling textiles. [71,72,73] And a small thickness of < ~150 μm is usually needed to maintain enough MIR transmittance, limiting the solar reflectivity (discussed in the following section) and mechanical strength. On the other hand, the performance of MIR-emissive textiles does not depend on the spectrum of the underlying surface and thus relaxes restrictions on thicknesses.[74,75] For example, $\bar{\varepsilon}_{LWIR}$ of 0.95 can be achieved through the hierarchical-morphology design of randomly dispersed scatterers throughout a metafabric. [76] Compared with PDRC films or paints, the woven structure enables metafabrics to easily accommodate complex deformations (bending, stretching, and twisting), which leads to versatile compatibility.

3.1.2. Selective emittance

As discussed above, various materials and structures with a strong thermal LWIR emittance have been investigated to achieve PDRC through the atmospheric LWIR window. However, most of the reported radiative cooling materials exhibit broadband absorptance/emittance, thereby covering the entire mid-infrared wavelength when the coating is facing the sky. Compared with a selective thermal emitter, a broadband thermal emitter with a high emittance beyond the atmospheric transmittance window absorbs downward thermal radiation from the atmosphere when the atmosphere temperature is higher than the coating, thereby compromising the cooling performance (Figure 9a).[77] Theoretical calculations show that an ideal selective emitter allows a larger temperature drop than that of the broadband

emitter (Figure 9b and c), especially when the coating temperature T_c is lower than the atmospheric temperature T_{amb}. Moreover, when $T_c = T_{amb}$, the PDRC performance between the selective emitter and non-selective emitter is similar because the absorbed radiation from the atmosphere is almost equal to the power emitted into the atmosphere.

In addition, the selective emitter is also significant at a vertically oriented coating because of the irradiation from the Earth glow, as shown in Figure 9d, wherein most of the surface area of typical buildings is vertically oriented and the ground temperature is higher.[34] Based on the differential transmittance or emittance of the atmosphere toward the sky (narrowband, LWIR) and between terrestrial objects (broadband), the selective emitter can reflect large bandwidths of broadband thermal radiation from the terrestrial object, even as they radiate and lose LWIR heat into the sky. Consequently, they can yield considerably greater cooling, which is then achieved by the broadband emitter (Figure 9e and f).

This type of selective emitter applies to various building envelopes, such as walls and windows, and can be conveniently produced from plastics, polymer resins, and ceramics. For example, poly(4-methyl-1-pentene) (PMP), poly(vinyl fluoride) (PVF), metalized polypropene (PP), biaxially oriented poly(ethene terephthalate) (BoPET), alumina (Al_2O_3) ceramic tiles, PMMA and PDMS-based paint resins, and common household materials such as scotch-tape, also exhibit selective LWIR emittance.[34] In addition, large-scalable fabrication technologies (such as paints for walls or electrospinning for textiles) have enabled substantial flexibility for the scalable manufacture of PDRC coatings in various applications.

3.1.3. Angle-dependent emittance

In addition to selective emittance properties, angle-dependent emittance is also of significant interest in PDRC applications. It's a fundamental challenge to control the directional emittance of far-field thermal radiation and photonic structures can be designed to achieve an angle-dependent emittance over narrow bandwidths. However, it's of significance to constrain

the thermal emittance over broad bandwidths to the specific angular range due to the broadband characteristics of thermal radiation in PDRC applications.

When the coating faces the sky, the temperature of surrounding buildings is higher than the emitter, as shown in Figure 10a. A broadband directional emitter was designed theoretically by covering an angular selector on the top of a broadband thermal emitter, as shown in Figure 10b. This type of directional emitter has high emittance with the emission angle ranging from 0 to 40° and nearly 100% reflectance from 40 to 90°, as shown in Figure 10c. Although the coating temperature can be decreased through PDRC coatings with an angular selector or not, the directional emitter exhibits better PDRC performance than the broadband emitter without an angular selector (Figure 10d).[78]

In addition, based on gradient epsilon-near-zero material, two broadband directional emitters were experimentally fabricated (Figure 10e and f). The angle-dependent emitters consisted of conventional oxides that exhibit high (> 0.7 and > 0.6) directional emittance (60–75° and 70–85°) in the broadband wavelength of 10.0–14.3 μm and 7.7–11.5 μm, respectively (Figure 10g and h). This broadband directional emitter enables meaningful heat transfer and energy applications, which can overcome the conventional limits on the angular response of selective emitter to improve performance in solar thermal conversion, thermophotovoltaics, radiative cooling, and waste heat recovery.[79]

3.2. Solar reflectance

In the daytime, the global solar irradiation heat flux at AM 1.5 is approximately 1000 W m^{-2},[9] which directly heats the coating facing the sky. In addition, the radiation power emitted to the cold outer space through the LWIR window by an ideal emitter at 25 °C only covers 10% of the solar intensity (100 W m^{-2}). Therefore, it is important to achieve an average solar reflectance $\bar{R}_{\text{solar}} > 0.9$, for PDRC applications.

Using highly reflective metal substrates (such as Ag and Al) underneath is a simple method to achieve $\bar{R}_{\text{solar}} > 0.9$ (Figure 11a).[4,18,19,32,51] Furthermore, the top materials in the coatings

should have low absorption ($k \sim 0$) in the solar spectrum and strong absorption in the atmospheric LWIR window. Thus, polymers (such as PDMS) or dielectric materials (such as Al_2O_3 and SiO_2) (Figure 6) can be coated on an Ag or Al reflector to achieve effective PDRC performance. However, the metal reflectors are usually smooth Ag or Al films, which would increase the costs of materials and manufacturing. Moreover, these metals are unstable in the air for long-term usage, especially in areas with high pollution or high humidity.

Solar reflectance can be improved by using Mie scattering while avoiding the use of metal reflectors. Thus, various dielectric microspheres (such as TiO_2[22,23], SiO_2[20,67], $CaCO_3$[80], and $BaSO_4$ [81]) or polymer microspheres (such as P(VdF-HFP) [70]) have been randomly stacked to investigate the PDRC performance (Figure 11b and c), and a high value of $\bar{R}_{\text{solar}} > 0.95$, could be achieved at a thickness of 300–500 μm by tuning the sphere parameters (such as material, size, and core-shell ratio).[52,42] However, some binders and thickeners are required to paint these random microsphere coatings, and the final product usually lacks flexible, water-repellent, and anti-abrasion properties, as discussed above.

A simple method to overcome the above problems is to mix these dielectric microspheres with polymers to achieve a high solar reflectance, as shown in Figure 11d. However, because of the similar refractive indices between dielectric microspheres and the polymer (such as 1.39 vs. 1.44 for PDMS and SiO_2), a large thickness (> 1000 μm) is usually needed to achieve $\bar{R}_{\text{solar}} > 0.9$. The $\bar{R}_{\text{solar}}$ of dielectric microsphere polymer coatings can be further improved by using metal reflectors [18] or hollow microspheres [82], or by mixing different microspheres [83,46]. Similarly, replacing microspheres with pores can greatly enhance the solar reflectance because it can introduce multi-size distributions and large differences in refractive index (such as 1.39 vs. 1.00 for P(VDF-HPF) vs. air), as shown in Figure 11e, leading to a high $\bar{R}_{\text{solar}} > 0.96$ at a thickness of 300 μm.[15,59,39,57] In addition, dielectric microspheres have also been added to the porous polymer coating (Figure 11f) to achieve a high solar reflectance by the coupling

scattering effect of multiple interfaces (such as dielectric-air, dielectric-polymer, and air-polymer).[55-47]

When the angle of incidence is larger than the critical angle, the incident light has reflected in the medium. This phenomenon is known as total internal reflectance, which occurs under the following two conditions: (1) the light moves from a denser medium to a less dense medium; (2) the angle of incidence is greater than the critical angle. Hence, the total internal reflectance was also introduced by modifying certain surface microstructures to further enhance the solar reflectance at a thinner thickness, as shown in Figures 11g and h. For the dielectric microsphere polymer coating (thickness is 500 μm) in Figure 11g, $\bar{R}_{\text{solar}}$ can increase from 0.29 to 0.96 by introducing a 3D architecture around the coating surface, which is attributed to the elimination of the pyramid photonic architectures and the smaller diameter of the Al_2O_3 particles suppress the effects of total internal reflectance and Mie scattering, respectively.[44] Furthermore, by applying micropores on the top of the porous PMMA coating to enhance the total internal reflectance, $\bar{R}_{\text{solar}}$ can be improved to 0.95, which is much higher than that of the nanopore PMMA coating ($\bar{R}_{\text{solar}}$ = 0.74), micropore PMMA coating ($\bar{R}_{\text{solar}}$ = 0.23), and pristine PMMA film ($\bar{R}_{\text{solar}}$ = 0.10) (Figure 11h).[31] In addition to coatings discussed above, a textile reflector based on PEO can achieve $\bar{R}_{\text{solar}}$ = 0.96, which scatters the solar irradiation by micro- and nanostructures (Figure 11i).[77]

As discussed above, the general strategies for achieving high solar reflectance can be divided into three categories: metal reflectors (such as Ag or Al), Mie scattering by spheres (such as dielectric spheres, polymer spheres, or voids), and total internal reflectance by surface microstructures (such as micropores, pyramids, and cones). The interface (such as SiO_2-polymer, SiO_2-air, air-polymer, $CaCO_3$-polymer, and TiO_2-polymer) in the coating can fully utilize Mie scattering to amplify solar scattering, which shows great potential in PDRC applications.

3.2. Colored PDRC coating

PDRC coatings need a high solar reflectance and thermal LWIR emittance to cool objects under sunlight. However, the white color of these coatings is very dazzling due to the high solar reflectance, which does not satisfy the need for color. The coloration of PDRC coatings would impair the cooling performance because of solar absorption in the visible spectrum. Hence, mitigating the solar absorption of the colored PDRC coating needs the narrowband selective absorption in the visible spectrum to balance the coloration and cooling performance.

Many research works have been conducted to achieve colored PDRC coatings. Theoretically, silicon nanostructures were designed to exhibit various colors based on the geometric design to achieve color-preserving PDRC (Figure 12a).[85] To further suppress the solar absorption of colored PDRC coatings in the visible spectrum, plasmonic Ag@SiO_2 core-shell nanoparticles (NPs) were embedded in the polymer matrix to achieve selective narrowband absorption in the visible spectrum (Figure 12b).[49] However, it is difficult to control the geometric parameters of these structural colors based on dielectric metasurfaces or plasmonic NPs, limiting their large-scale usage and applications.

A paintable bilayer coating was prepared to achieve colored PDRC coating to overcome this problem (Figure 12c). The top layer absorbs appropriate visible wavelengths to display specific colors by dyes, while the underlayer enhances the reflectance of near-infrared light to reduce solar heating.[22] In addition, recent innovations such as fluorescent pigments that convert visible absorption to NIR emission, instead of the light-to-heat conversion in the colored PDRC coating to reduce the effect of coloration on the cooling performance. For example, bilayer-colored PDRC coatings were also prepared using silica-embedded perovskite nanoparticles on a highly mid-infrared-radiative white emitter (Figure 12d). [86] These results indicate that the bilayer paintable coating based on fluorescent pigments can achieve both coloration and PDRC in large-scale production, inexpensive, and great applicability manner.

3.3. Dynamic switchable radiative cooling coatings

Daytime and nighttime radiative cooling by reflecting solar irradiation (0.3–2.5 μm) and emitting mid-infrared radiation through the LWIR atmospheric window (8–13 μm) has been extensively investigated in recent decades. However, in some applications (such as roofs in the temperate zone), cooling is preferred in summer but not desired in winter for better thermal comfort. To overcome this issue, dynamically switchable coatings have been developed to prevent overcooling in winter or cold environments, which can be divided into several categories based on: (1) temperature (Figure 13a), (2) dielectric environment (Figure 13b), and (3) mechanical force (Figure 13c to e).

The operational mode of a temperature-dependent switchable coating can be controlled based on the critical temperature T_{ct} of the phase change material. When $T_c > T_{ct}$, the coating operates as a cooling device, and when $T_c < T_{ct}$, the coating stays in the heating mode. Switchable coatings based on vanadium dioxide (VO_2), [87-91] which exhibit an insulator-to-metal transition at T_{ct} = 68 °C, have been developed.[92] For example, a self-adaptive coating based on VO_2 was theoretically designed; the coating can adaptively turn "on" and "off" radiative cooling in the LWIR atmospheric window while the solar reflectance is unchanged ($\bar{R}_{solar} \sim 1$) by a spectrally selective filter, depending on the ambient temperature without any extra energy input for switching, as shown in Figure 13a.[89] In addition to the switchable emittance in the LWIR atmospheric window, a hybrid VO_2/TiN coating was prepared to dynamically control near-infrared (IR) radiation based on the ambient temperature and solar intensity.[93] Solar heating by plasmonic TiN can reduce the transition ambient temperature, making VO_2/TiN promising as a smart energy-saving coating in buildings. For temperature-dependent coatings, choosing a suitable phase change material is critical for different applications owing to the various T_{cr} values. Much effort has been devoted to VO_2 coatings in the switching of the mid-infrared spectrum, and only a few studies have reported the switchable ability of temperature-dependent coatings in the solar spectrum.

Apart from temperature-dependent switchable coatings, other dynamic switchable coatings require extra energy input for switching. One method for developing such dynamic coatings is to change the dielectric environment. For example, based on reversible wetting with common liquids (such as water and alcohol) and drying, the transmittances of porous polymer coatings can be switched as exemplified by P(VdF-HFP) switching from white to transparent (ΔT_{solar} = 0.74) and PE switching from a greenhouse (ΔT_{solar} = 0.33 and ΔT_{LWIR} = 0.64) (Figure 13b).[94] These coatings based on reversible wetting can achieve switchable sub-ambient radiative cooling by 3.2 °C and above-ambient solar heating by 21.4 °C. The switching mechanism is similar to that discussed above in the solar reflectance of porous polymer coatings due to the difference in refractive indices at the interfaces of air-polymer, liquid-polymer, or dielectric environments of porous coatings, which have also been widely applied in color switchable display coatings by changing different liquids with various refractive indices.[95] For the dielectric environment-dependent coating, the recycling, and utilization of working liquids and the tightness of the circulation loop should be considered in realistic applications.

Another method to switch the optical properties of a coating is based on mechanical force, which has been widely investigated in polymer coatings owing to their stretchability. For example, a switching strategy was reported based on the dynamic cavitation of PDMS coatings that can be reversibly and continuously tuned from a highly porous state ($\bar{R}_{solar}$ = 0.93 for cooling) to a transparent solid ($\bar{R}_{solar}$ = 0.05), while $\bar{\varepsilon}_{LWIR}$ = 0.94, with little change due to the high absorptance of PDMS at a large thickness (Figure 13c).[50] To achieve a switchable coating in $\bar{\varepsilon}_{LWIR}$, mechanical stress/strain can be applied in a thin PDMS film, consisting of a PDMS grating and embdeded nanoparticles (Figure 13d). A dynamic tuning in $\bar{\varepsilon}_{LWIR}$ under different strains resulted in a continuously variable "ON"/"OFF" mode in the atmospheric LWIR window while $\bar{R}_{solar}$ = 0.9 with little changes due to the bottom Ag reflector.[96] To achieve switching in both $\bar{R}_{solar}$ and $\bar{\varepsilon}_{LWIR}$, a simple switchable device was designed based on a

selective solar absorber (Cu-Zn) for heating and a PDRC coating (PDMS-Ag) for cooling by switching the two coatings (Figure 13e).[97] Based on this switchable coating, 19.2% of the energy used for heating and cooling can be saved in the U.S., which is 1.7 times higher than the only cooling mode and 2.2 times higher than the only heating mode.

As discussed above, temperature-dependent switchable coatings without any extra energy input for switching are of great interest, and it is critical to choose suitable phase-change materials based on the demanded transition temperature and spectral response in the solar spectrum or LWIR atmospheric window. Moreover, the optical response of switchable coatings can be easily controlled by dielectric-environment- or mechanical force-dependent coatings. However, it should be noted that the response spectra must be considered for different applications. For example, in the daytime, solar heating is critical for thermal management, and more attention should be paid to the solar spectrum for switching. For nighttime performance, more efforts should be made in improving the LWIR atmospheric window.

4. Applications and Challenges of PDRC

Various PDRC materials or structures have been designed with appealing optical properties; however, the design of the cooling system needs to consider several important problems, including the system configuration and controls, cooling load profiles from end-users, the impact of weather conditions, the system cost and payback period. Radiative cooling in the daytime is a potential direction to mitigate the energy crisis, and its application has attracted considerable interest in recent years. In this section, we review some applications of PDRC, such as space cooling, solar cell cooling, harvesting water from the atmosphere, and electricity generation.

4.1. Space cooling

Space cooling (such as for buildings, cargo boxes, and cars) consumes a significant amount of energy. For example, the energy used to run air conditioners and electric fans for cooling

account for approximately 10% of the total global electricity.[98] Under favorable climates, PDRC can supply ~ 80% of the cooling load of residential buildings.[8,99]

The first way to apply PDRC is to directly apply a passive PDRC coating on a terrestrial entity that needs to be cooled, such as the cooling roof is shown in Figure 14a.[99–109] Roofs in most residential buildings are exposed to substantial solar radiation during the daytime, resulting in a high roof temperature (up to 60 °C). This heat is transferred to the living space, placing a higher cooling load on the air conditioner. PDRC coatings directly covering the roof reflect a large portion of solar radiation and achieve a lower roof temperature, which can reduce cooling loads by 18–93%.[100,101] For example, as shown in Figure 14b, the cooling load savings are generally higher than the heating load, resulting in positive annual energy savings. The cities of Kunming, Hong Kong, Shanghai, Beijing, and Harbin can achieve energy saving rates of 9.3%, 7.1%, 4.1%, 3.3%, and 0.6% due to the different climates. [109]

Even though the cooling in the winter period would increase the energy input while the cooling load savings surpassed the heating load penalties. A cool roof can save annual cooling energy of 33-57 USD m^{-2} for the top-floor residential units with a short payback period (< 6 months). [110] The annual direct CO_2 reductions are estimated to be 11–12 kg CO_2 m^{-2}.[103,111] The typical energy savings ranged from 0.1 to 8.6 kWh m^{-2}, 1.1 to 8.2 kWh $m^{-2,}$ and 1.4 to 10.9 kWh m^{-2} for residential, office, and retail buildings, respectively based on cool roof applications in the U.S.[112] These results indicate that the PDRC coating applied to the roof presents a potential energy-saving way especially for buildings in Hot-Summer-Warm-Winter (HSWW) and temperate climatic regions where much cooling load is required.

The second approach is to develop an active system. In active systems, a heat transfer fluid is used for space cooling, which is better controlled and more feasible to regulate cooling power, as shown in Figures 14c and d. [113] However, these systems are more complicated, and external energy (fan or pump) is needed to transfer fluids or air for cooling. Active systems integrating

PDRC with other energy systems (such as photovoltaic-thermal,[114,115] HVAC,[116,117], and thermoelectric (TE) cooling systems [118]) include air-based,[98,106] open or closed-loop water-based,[113,119] and hybrid systems.[120,121]

Water-based cooling systems can be categorized into open-loop, [122] and closed-loop systems.[123] The closed-loop water system utilizes water as a heat transfer fluid and dissipates the heat by a flat-plate cooling radiator, which is different from an open-loop water system, which dissipates heat through convection, radiation, and evaporation, transferring the heat from the roof to the surrounding environment through the water in the roof pond. The average net cooling power of water-based systems is usually higher than that of air-based systems.[119,124] However, the advantage of air-based systems is that they can provide instantaneous cooling to buildings at night using fans or driven by buoyancy forces. To combine the advantages of the above two systems, a hybrid diurnal radiative cooled-cold storage cooling system was designed, which can save 26% ~ 46% of annual cooling electricity with an 8-year payback period.[120]

4.2. Solar cell cooling

Thermal management is also important for device operation. For example, an increased operating temperature not only reduces the efficiency of photovoltaic systems but also greatly reduces their lifetimes.[125] Generally, the negative temperature coefficient of silicon solar cells is approximately 0.45%, which means that the efficiency of a Si-based solar cell (with 22% efficiency) decreases by approximately 0.1% when the temperature increases by 1°C.[126] Further research shows that the actual effective spectral range of Si-based solar cells is within 0.3–1.1 μm, while the rest of the solar energy is converted into heat, which further reduces the conversion efficiency of solar cells. Therefore, thermal management is essential in photovoltaic systems. In contrast to space cooling, the operating temperature of solar cells is higher than the ambient temperature; therefore, there is no need to suppress nonradiative heat transfer, which is beneficial to the heat dissipation for solar cells. Meanwhile, the emittance of Si-based solar

cells can reach 85% in the LWIR transmission window because of the large absorption dip of Si near the wavelength of 9 μm.[127]

Therefore, one approach is to design a special PDRC coating that can radiate heat strongly through thermal emission and can also significantly reflect the solar radiation in the sub-band-gap and ultraviolet regimes (Figure 15a). Applying this cooler to a solar panel has been experimentally shown to reduce the Si-based cell temperature by over 5.7 °C.[128] However, it has thus far been difficult to commercialize photonic selectively reflecting structures because of the cost and immature processing technology of photonic structures. Another approach is to using PDRC to remove excess waste heat from solar cells is straightforward, and can be achieved by placing a thin-layer PDRC coating.[129-131] For example, a direct method to apply a common PDRC coating on top of the solar cells (Figure 15b) was reported. A temperature drop of 36 °C for concentration photovoltaic was demonstrated experimentally, leading to a 27% increase in the open-circuit voltage for GaSb cells and a predicted lifetime extension of 4 to 15 times.[132]

4.3. Harvesting water from the atmosphere

Due to population growth and industrial development, the availability of fresh water has become a serious problem in arid and humid areas of the world.[133] Utilizing radiative cooling coatings to harvest more water from the atmosphere can relieve the problem without any energy input.[134] Dew collection technology uses an ultracold outer space to radiatively cool a surface below the dew point and condenses water vapor from the atmosphere. This passive technology has great potential for freshwater harvesting because of the significant amount of water vapor stored in the atmosphere.

Compared to convective condensers, the daytime radiative condenser utilizes both convection and radiation for cooling and thus can substantially improve the condensation rate, as shown in Figures 16a and b. For example, at the most favorable condition for the convective condenser (black solid line in Figure 16c), the condensation rate of the radiative condenser

almost doubles that of the convective condenser, reaching 2.5 L m^{-2} h^{-1} (red solid curve in Figure 16c), well above the theoretical limit of the one-sun evaporation rate.[135] Such a high condensation rate will also increase the vapor pressure gradient inside the water-harvesting system, further facilitating the water-production cycle.

To improve the PDRC condenser performance, research has been widely conducted on condenser coatings,[136,137,138,139,] and meteorological parameters.[140,141] The upper limit of the performance of this technology was calculated theoretically as shown in Figure 16d.[141] When a blackbody emitter is used, a condenser consisting of a selective emitter can condense water vapor under highly arid conditions. In addition, multifunctional coatings that are favorable for both droplet nucleation and removal are also highly desirable for harvesting water from the atmosphere. For example, a hydrophilic directional slippery rough surface was developed for rapid droplet nucleation and water removal, as shown in Figure 16e.[142] Coupling the PDRC performance with multifunctional surfaces can motivate the development of better radiative coolers for dew-harvesting applications.

4.4. Electricity generation

The ability of the PDRC coating to passively maintain a surface below ambient air temperature is also useful for electricity generation, which converts the temperature difference into usable electricity based on a TE generator. TE generators have attracted great attention in the past two decades to recover usable power from waste heat or solar heating.[143,144] In contrast, PDRC technology can provide a cold source and integrate with the TE model to generate electricity, which is unlike traditional TE generators.

The cooling effect in PDRC can be combined with TE to generate electricity at night when photovoltaic systems do not work. Generating electricity at night can be used in a wide range of applications, such as sensors and lighting. For example, a commercial TE generator was combined with the radiative cooling coating at night experimentally to achieve a power generation of 25 mW m^{-2}, which can be used to the lighting in the dark space (Figure 17a).[145]

Furthermore, an high electrical power density > 2 W m^{-2} was achieved using a spectro-angular-selective emitter (Figure 17b),[146] which was close to the Carnot thermodynamic limit. These results show that it's significant to optimize the emitter to enhance the power density for electricity generation based on radiative cooling.

Another way is to generate electricity throughout the day based on TE, as shown in Figure 17c.[147] A selective emitter (high reflectance/low emittance in the solar spectrum and high emittance in the atmospheric LWIR window) is placed on the TE device. And the top surface of the TE generator is always cooled due to the PDRC all the time. Therefore, continuous TE generation was maintained. On the contrary, if a broadband emitter (high emittance/absorptance in both solar spectrum and atmospheric LWIR window) is placed on the TE device, the broadband emitter will be heated in the daytime by solar absorption while be cooled in the nighttime by thermal radiation through the atmospheric window. Hence, the top temperature gradually increases from night to morning and the temperature difference will become zero, which also can be observed as the time shifts from day to evening. At these moments, the output of the TE generation becomes zero. In addition, the weather changes, such as clouds, also would reduce the output to zero. Therefore, for continuous electricity generation based on radiative cooling, the temperature difference generated in the daytime should be considered cautiously from the stable electricity generation, sign change and electric/voltage intensity based on different applications.

4.5. Challenges

In addition to the applications discussed above, other PDRC applications (such as water cooling,[36] power plant condenser cooling,[148] and human body cooling [149,150]) have also gained considerable attention. However, the commercialization of PDRC technologies has many potential challenges that need to be considered, such as climate, cost, performance, and durability.

To identify the effect of climates on the large-scale deployment of PDRC, a world map of annual PDRC potential is shown in Figure 18. The PDRC potential is dependent on the location due to the regional climates.[24] A dry and hot climate is good for the PDRC applications with a higher cooling power of > 120 W m^{-2}. On the contrary, A cold, highly humid, or cloudy climate would lead to a much lower cooling potential. The wide adoption of PDRC materials in regions with high cooling potentials not only improves building thermal management both day and night but also reduces the extra structure for roof insulation or solar shading in these areas.

Low cost is an important factor and is related to low-cost materials and easy availability and manufacturing processes. Employing precious metals (Ag or Al) as solar reflective layers, complex manufacturing processes, as well as valuable materials, would increase the cost. Polymers have gained considerable attention because of their price advantage. However, to meet different applications, the design of polymer-based PDRC coatings still requires further research, and most PDRC coatings can improve their cooling performance through structural optimization. The low cooling power density of PDRC requires large areas to meet the cooling load, which also increases the cost of the PDRC system. Simultaneously, the durability and stability of PDRC materials are also an important challenge. Various aspects should be considered for durabilities, such as stability against moisture, oxygen, ultraviolet light, and dust. For polymer-based coatings, it is difficult to maintain high solar reflectance because of the degradation of the polymer and metal solar-reflective layer. Transparent varnishes can be covered above the cooling coating to alleviate this problem.[12] In addition, waste management/disposal, low energy density, and mechanical stability must be considered in practical applications.

5. Conclusion

PDRC technologies that do not consume external energy have evolved rapidly in recent years and have gained considerable attention in both scientific and industrial communities.

Scalable-manufactured PDRC coatings, such as paintings, can be applied on a large scale. Simultaneously, the performance of PDRC can be further improved by geometric optimization or system engineering. Furthermore, the integration of PDRC with new functionalities, such as a wide range of colors, switchable and self-cleaning properties, could help to expand PDRC applications. PDRC technologies have been widely applied for space cooling, removing excess waste heat from solar cells, harvesting water from the atmosphere, and generating electricity. However, performances other than cooling performance, such as cost, durability, and low energy density, should also be considered in real applications. With the increasing energy and environmental challenges, PDRC shows great potential for reducing the energy consumption of cooling, alleviating the urban heat island effect, and solving water and environmental problems soon.

Acknowledgments

M. C. would like to acknowledge the financial support from the Central South University and the National Natural Science Foundation of China (Grant No. 52006246). Y.Y. acknowledges support from the National Science Foundation (Award No. 2005747)

Conflict of interest

The authors declare no conflict of interest.

References

1. Hanif M, Mahlia TMI, Zare A, Saksahdan TJ, Metselaar HSC. Potential energy savings by radiative cooling system for a building in tropical climate. *Renew Sustain Energy Rev*. 2014;32:642-650. doi:10.1016/j.rser.2014.01.053
2. Santamouris M. Innovating to zero the building sector in Europe: Minimising the energy consumption, eradication of the energy poverty and mitigating the local climate change. *Sol Energy*. 2016;128:61-94. doi:10.1016/j.solener.2016.01.021

3. Chen M, He Y, Hu Y, Zhu J. Local temperature control of hybrid plasmonic nano-antennas. *J Quant Spectrosc Radiat Transf*. 2019;225:50-57. doi:10.1016/j.jqsrt.2018.12.023

4. Raman AP, Anoma MA, Zhu L, Rephaeli E, Fan S. Passive radiative cooling below ambient air temperature under direct sunlight. *Nature*. 2014;515(7528):540-544. doi:10.1038/nature13883

5. Liu J, Zhou Z, Zhang D, et al. Research on the performance of radiative cooling and solar heating coupling module to direct control indoor temperature. *Energy Convers Manag*. 2020;205:112395. doi:10.1016/j.enconman.2019.112395

6. Fixsen DJ. The temperature of the cosmic microwave background. *Astrophys J*. 2009;707(2):916-920. doi:10.1088/0004-637X/707/2/916

7. Zhao B, Hu M, Ao X, Chen N, Pei G. Radiative cooling: A review of fundamentals, materials, applications, and prospects. *Appl Energy*. 2019;236:489-513. doi:10.1016/j.apenergy.2018.12.018

8. Zeyghami M, Goswami DY, Stefanakos E. A review of clear sky radiative cooling developments and applications in renewable power systems and passive building cooling. *Sol Energy Mater Sol Cells*. 2018;178(August 2017):115-128. doi:10.1016/j.solmat.2018.01.015

9. Eriksson TS, Granqvist CG. Radiative cooling computed for model atmospheres. *Appl Opt*. 1982;21(23):4381. doi:10.1364/ao.21.004381

10. Granqvist CG. Radiative heating and cooling with spectrally selective surfaces. *Appl Opt*. 1981;20(15):2606. doi:10.1364/ao.20.002606

11. Rephaeli E, Raman A, Fan S. Ultrabroadband photonic structures to achieve high-performance daytime radiative cooling. *Nano Lett*. 2013;13(4):1457-1461. doi:10.1021/nl4004283

12. Yang Y, Zhang Y. Passive daytime radiative cooling: Principle, application, and economic analysis. *MRS Energy Sustain*. 2020;7:1-8. doi:10.1557/mre.2020.18

13. Zhao D, Aili A, Zhai Y, et al. Radiative sky cooling: Fundamental principles, materials, and applications. *Appl Phys Rev*. 2019;6(2):021306. doi:10.1063/1.5087281

14. Liu J, Zhou Z, Zhang D, et al. Field investigation and performance evaluation of sub-ambient radiative cooling in low latitude seaside. *Renew Energy*. 2020;155:90-99. doi:10.1016/j.renene.2020.03.136

15. Mandal J, Fu Y, Overvig AC, et al. Hierarchically porous polymer coatings for highly efficient passive daytime radiative cooling. *Science (80-)*. 2018;362(6412):315-319. doi:10.1126/science.aat9513

16. Jeong SY, Tso CY, Ha J, et al. Field investigation of a photonic multi-layered TiO2 passive radiative cooler in sub-tropical climate. *Renew Energy*. 2020;146:44-55. doi:10.1016/j.renene.2019.06.119

17. Yalçın RA, Blandre E, Joulain K, Drévillon J. Daytime radiative cooling with silica fiber network. *Sol Energy Mater Sol Cells*. 2020;206:110320. doi:10.1016/j.solmat.2019.110320

18. Zhai Y, Ma Y, David SN, et al. Scalable-manufactured randomized glass-polymer hybrid metamaterial for daytime radiative cooling. *Science (80-)*. 2017;355(6329):1062-1066. doi:10.1126/science.aai7899

19. Chen Z, Zhu L, Raman A, Fan S. Radiative cooling to deep sub-freezing temperatures through a 24-h day-night cycle. *Nat Commun*. 2016;7:13729. doi:10.1038/ncomms13729

20. Atiganyanun S, Plumley JB, Han SJ, et al. Effective Radiative Cooling by Paint-Format Microsphere-Based Photonic Random Media. *ACS Photonics*. 2018;5(4):1181-1187. doi:10.1021/acsphotonics.7b01492

21. Bao H, Yan C, Wang B, Fang X, Zhao CY, Ruan X. Double-layer nanoparticle-based coatings for efficient terrestrial radiative cooling. *Sol Energy Mater Sol Cells*. 2017;168:78-84. doi:10.1016/j.solmat.2017.04.020

22. Chen Y, Mandal J, Li W, et al. Colored and paintable bilayer coatings with high solar-infrared reflectance for efficient cooling. *Sci Adv*. 2020;6(17):eaaz5413. doi:10.1126/sciadv.aaz5413

23. Huang Z, Ruan X. Nanoparticle embedded double-layer coating for daytime radiative cooling. *Int J Heat Mass Transf*. 2017;104:890-896. doi:10.1016/j.ijheatmasstransfer.2016.08.009

24. Yin X, Yang R, Tan G, Fan S. Terrestrial radiative cooling: Using the cold universe as a renewable and sustainable energy source. *Science (80-)*. 2020;370(6518):786-791. doi:10.1126/science.abb0971

25. Yu X, Chan J, Chen C. Review of radiative cooling materials: Performance evaluation and design approaches. *Nano Energy*. 2021;88:106259. doi:10.1016/j.nanoen.2021.106259

26. Lin K Te, Han J, Li K, Guo C, Lin H, Jia B. Radiative cooling: Fundamental physics, atmospheric influences, materials and structural engineering, applications and beyond. *Nano Energy*. 2021;80:105517. doi:10.1016/j.nanoen.2020.105517

27. Li Z, Chen Q, Song Y, Zhu B, Zhu J. Fundamentals, Materials, and Applications for Daytime Radiative Cooling. *Adv Mater Technol*. 2020;32(42):1906752. doi:10.1002/admt.201901007

28. Santamouris M, Feng J. Recent progress in daytime radiative cooling: Is it the air conditioner of the future? *Buildings*. 2018;8(12). doi:10.3390/buildings8120168

29. Zhu L, Raman AP, Fan S. Radiative cooling of solar absorbers using a visibly transparent photonic crystal thermal blackbody. *Proc Natl Acad Sci U S A*. 2015;112(40):12282-12287. doi:10.1073/pnas.1509453112

30. Song J, Seo J, Han J, Lee J, Lee BJ. Ultrahigh emissivity of grating-patterned PDMS film from 8 to 13 μ m wavelength regime. *Appl Phys Lett*. 2020;117(9). doi:10.1063/5.0017838

31. Wang T, Wu Y, Shi L, Hu X, Chen M, Wu L. A structural polymer for highly efficient all-day passive radiative cooling. *Nat Commun*. 2021;12(1):1-11. doi:10.1038/s41467-020-20646-7

32. Zhou L, Song H, Liang J, et al. A polydimethylsiloxane-coated metal structure for all-day radiative cooling. *Nat Sustain*. 2019;2(8):718-724. doi:10.1038/s41893-019-0348-5

33. Aili A, Wei ZY, Chen YZ, Zhao DL, Yang RG, Yin XB. Selection of polymers with functional groups for daytime radiative cooling. *Mater Today Phys*. 2019;10:100127. doi:10.1016/j.mtphys.2019.100127

34. Mandal J, Mandal S, Brewer J, Ramachandran A, Raman AP. Radiative Cooling and Thermoregulation in the Earth's Glow. *arXiv*. Published online 2020:1-13.

35. Zhu R, Hu D, Chen Z, et al. Plasmon-Enhanced Infrared Emission Approaching the Theoretical Limit of Radiative Cooling Ability. *Nano Lett*. 2020;20(10):6974-6980. doi:10.1021/acs.nanolett.0c01457

36. Zhao D, Aili A, Zhai Y, et al. Subambient Cooling of Water: Toward Real-World Applications of Daytime Radiative Cooling. *Joule*. 2019;3(1):111-123. doi:10.1016/j.joule.2018.10.006

37. Kou J long, Jurado Z, Chen Z, Fan S, Minnich AJ. Daytime Radiative Cooling Using Near-Black Infrared Emitters. *ACS Photonics*. 2017;4(3):626-630. doi:10.1021/acsphotonics.6b00991

38. Gamage S, Banerjee D, Alam MM, et al. Reflective and transparent cellulose-based passive radiative coolers. *Cellulose*. Published online 2021. doi:10.1007/s10570-021-04112-1

39. Leroy A, Bhatia B, Kelsall CC, et al. High-performance subambient radiative cooling enabled by optically selective and thermally insulating polyethylene aerogel. *Sci Adv*. 2019;5(10):eaat9480. doi:10.1126/sciadv.aat9480

40. Jaramillo-Fernandez J, Whitworth GL, Pariente JA, et al. A Self-Assembled 2D Thermofunctional Material for Radiative Cooling. *Small*. 2019;15(52):1-9. doi:10.1002/smll.201905290

41. Lee E, Luo T. Black body-like radiative cooling for flexible thin-film solar cells. *Sol Energy Mater Sol Cells*. 2019;194(August 2018):222-228. doi:10.1016/j.solmat.2019.02.015

42. Suichi T, Ishikawa A, Tanaka T, Hayashi Y, Tsuruta K. Whitish daytime radiative cooling using diffuse reflection of non-resonant silica nanoshells. *Sci Rep*. 2020;10(1):1-6. doi:10.1038/s41598-020-63591-7

43. Blandre E, Yalçin RA, Joulain K, Drévillon J. Microstructured surfaces for colored and non-colored sky radiative cooling. *Opt Express*. 2020;28(20):29703. doi:10.1364/oe.401368

44. Zhang H, Ly KCS, Liu X, et al. Biologically inspired flexible photonic films for efficient passive radiative cooling. *Proc Natl Acad Sci U S A*. 2020;117(26):14657-14666. doi:10.1073/pnas.2001802117

45. Li X, Peoples J, Huang Z, Zhao Z, Qiu J, Ruan X. Full Daytime Sub-Ambient Radiative Cooling with High Figure of Merit in Commercial-Like Paints. *SSRN Electron J*. Published online 2020. doi:10.2139/ssrn.3652325

46. Cheng ZM, Shuai Y, Gong DY, Wang FQ, Liang HX, Li GQ. Optical properties and cooling performance analyses of single-layer radiative cooling coating with mixture of TiO2 particles and SiO2 particles. *Sci China Technol Sci*. 2021;64(5):1017-1029. doi:10.1007/s11431-020-1586-9

47. Wang X, Liu X, Li Z, et al. Scalable Flexible Hybrid Membranes with Photonic Structures for Daytime Radiative Cooling. *Adv Funct Mater*. 2020;30(5):1907562. doi:10.1002/adfm.201907562

48. Ziming C, Fuqiang W, Dayang G, Huaxu L, Yong S. Low-cost radiative cooling blade coating with ultrahigh visible light transmittance and emission within an "atmospheric window." *Sol Energy Mater Sol Cells*. 2020;213:110563. doi:10.1016/j.solmat.2020.110563

49. Yalçln RA, Blandre E, Joulain K, Drévillon J. Colored Radiative Cooling Coatings with Nanoparticles. *ACS Photonics*. 2020;7(5):1312-1322. doi:10.1021/acsphotonics.0c00513

50. Zhao H, Sun Q, Zhou J, Deng X, Cui J. Switchable Cavitation in Silicone Coatings for Energy-Saving Cooling and Heating. *Adv Mater*. 2020;32(29):2000870. doi:10.1002/adma.202000870

51. Chae D, Kim M, Jung PH, et al. Spectrally Selective Inorganic-Based Multilayer Emitter for Daytime Radiative Cooling. *ACS Appl Mater Interfaces*. 2020;12(7):8073-8081. doi:10.1021/acsami.9b16742

52. Nie X, Yoo Y, Hewakuruppu H, Sullivan J, Krishna A, Lee J. Cool White Polymer Coatings based on Glass Bubbles for Buildings. *Sci Rep*. 2020;10(1):1-10. doi:10.1038/s41598-020-63027-2

53. Zhang X, Yang L, Wang F, Cheng Z, Liang H. Wrinkled surface microstructure for enhancing the infrared spectral performance of radiative cooling. *Opt Express*. 2021;29(8):11416. doi:10.1364/oe.418650

54. Zhong S, Yi L, Zhang J, et al. Self-cleaning and spectrally selective coating on cotton fabric for passive daytime radiative cooling. *Chem Eng J*. 2021;407(March 2020):127104. doi:10.1016/j.cej.2020.127104

55. Xiang B, Zhang R, Luo Y, et al. 3D porous polymer film with designed pore architecture and auto-deposited SiO2 for highly efficient passive radiative cooling. *Nano Energy*. 2021;81:105600. doi:10.1016/j.nanoen.2020.105600

56. Zhou K, Li W, Patel BB, et al. Three-Dimensional Printable Nanoporous Polymer Matrix Composites for Daytime Radiative Cooling. *Nano Lett*. 2021;21(3):1493-1499. doi:10.1021/acs.nanolett.0c04810

57. Zhang J, Zhou Z, Tang H, et al. Mechanically Robust and Spectrally Selective Convection Shield for Daytime Subambient Radiative Cooling. *ACS Appl Mater Interfaces*. 2021;13(12):14132-14140. doi:10.1021/acsami.0c21204

58. Feng C, Yang P, Liu H, et al. Bilayer porous polymer for efficient passive building cooling. *Nano Energy*. 2021;85:105971. doi:10.1016/j.nanoen.2021.105971

59. Chen M, Pang D, Mandal J, et al. Designing Mesoporous Photonic Structures for High-Performance Passive Daytime Radiative Cooling. *Nano Lett*. 2021;21(3):1412–1418. doi:10.1021/acs.nanolett.0c04241

60. Chae D, Son S, Lim H, Jung P-H, Ha J, Lee H. Scalable and Paint-format Microparticle–polymer Composite Enabling High-performance Daytime Radiative Cooling. *Mater Today Phys*. Published online 2021:100389. doi:10.1016/j.mtphys.2021.100389

61. Zhu Y, Ye YH, Wang D, Cao Y. Quasi-periodic selective multilayer emitter for sub-ambient daytime radiative cooling. *AIP Adv*. 2021;11(2):025109. doi:10.1063/5.0035138

62. Kitamura R, Pilon L, Jonasz M. Optical constants of silica glass from extreme ultraviolet to far infrared at near room temperature. *Appl Opt*. 2007;46(33):8118-8133. doi:10.1364/AO.46.008118

63. Kischkat J, Peters S, Gruska B, et al. Mid-infrared optical properties of thin films of aluminum oxide, titanium dioxide, silicon dioxide, aluminum nitride, and silicon nitride. *Appl Opt*. 2012;51(28):6789-6798. doi:10.1364/AO.51.006789

64. Siefke T, Kroker S, Pfeiffer K, et al. Materials Pushing the Application Limits of Wire Grid Polarizers further into the Deep Ultraviolet Spectral Range. *Adv Opt Mater*. 2016;4(11):1780-1786. doi:10.1002/adom.201600250

65. Zhang X, Qiu J, Zhao J, Li X, Liu L. Complex refractive indices measurements of polymers in infrared bands. *J Quant Spectrosc Radiat Transf*. 2020;252:107063. doi:10.1016/j.jqsrt.2020.107063

66. Sultanova N, Kasarova S, Nikolov I. Dispersion properties of optical polymers. *Acta Phys Pol A*. 2009;116(4):585-587. doi:10.12693/APhysPolA.116.585

67. Chen M, Pang D, Chen X, Yan H. Investigating the effective radiative cooling performance of random dielectric microsphere coatings. *Int J Heat Mass Transf*. 2021;173:121263. doi:10.1016/j.ijheatmasstransfer.2021.121263

68. Chen M, Pang D, Chen X, Yan H. Enhancing infrared emission behavior of polymer coatings for radiative cooling applications. *J Phys D Appl Phys*. 2021;54(29):295501. doi:10.1088/1361-6463/abfb19

69. Weng Y, Zhang W, Jiang Y, Zhao W, Deng Y. Effective daytime radiative cooling via a template method based PDMS sponge emitter with synergistic thermo-optical activity. *Sol Energy Mater Sol Cells*. 2021;230:111205. doi:10.1016/j.solmat.2021.111205

70. Huang W, Chen Y, Luo Y, et al. Scalable Aqueous Processing-Based Passive Daytime Radiative Cooling Coatings. *Adv Funct Mater*. 2021;2010334:1-7. doi:10.1002/adfm.202010334

71. Hsu PC, Li X. Photon-engineered radiative cooling textiles. *Science (80-)*. 2020;370(6518):784-785. doi:10.1126/science.abe4476

72. Peng Y, Chen J, Song AY, et al. Nanoporous polyethylene microfibres for large-scale radiative cooling fabric. *Nat Sustain*. 2018;1(2):105-112. doi:10.1038/s41893-018-0023-2

73. Kim H, McSherry S, Brown B, Lenert A. Selectively Enhancing Solar Scattering for Direct Radiative Cooling through Control of Polymer Nanofiber Morphology. *ACS Appl Mater Interfaces*. 2020;12(39):43553-43559. doi:10.1021/acsami.0c09374

74. Zhang XA, Yu S, Xu B, et al. Dynamic gating of infrared radiation in a textile. *Science (80-)*. 2019;363(6427):619-623. doi:10.1126/science.aau1217

75. Shi NN, Tsai CC, Carter MJ, et al. Nanostructured fibers as a versatile photonic platform: Radiative cooling and waveguiding through transverse Anderson localization. *Light Sci Appl*. 2018;7(1):1-9. doi:10.1038/s41377-018-0033-x

76. Zeng S, Pian S, Su M, et al. Hierarchical-morphology metafabric for scalable passive daytime radiative cooling. *Science (80-)*. 2021;373(6555):692-696. doi:10.1126/science.abi5484

77. Li D, Liu X, Li W, et al. Scalable and hierarchically designed polymer film as a selective thermal emitter for high-performance all-day radiative cooling. *Nat Nanotechnol*. 2021;16(2):153-158. doi:10.1038/s41565-020-00800-4

78. Qu Y, Pan M, Qiu M. Directional and spectral control of thermal emission and its application in radiative cooling and infrared light sources. *Phys Rev Appl*. 2020;13(6):064052. doi:10.1103/PhysRevApplied.13.064052

79. Xu J, Mandal J, Raman AP. Broadband directional control of thermal emission. *Science (80-)*. 2021;372(6540):393-397. doi:10.1126/science.abc5381

80. Li X, Peoples J, Huang Z, Zhao Z, Qiu J, Ruan X. Full Daytime Sub-ambient Radiative Cooling in Commercial-like Paints with High Figure of Merit. *Cell Reports Phys Sci*. 2020;1(10):100221. doi:10.1016/j.xcrp.2020.100221

81. Li X, Peoples J, Yao P, Ruan X. Ultrawhite BaSO4Paints and Films for Remarkable Daytime Subambient Radiative Cooling. *ACS Appl Mater Interfaces*. 2021;13(18):21733-21739. doi:10.1021/acsami.1c02368

82. Yu Z, Nie X, Yuksel A, Lee J. Reflectivity of solid and hollow microsphere composites and the effects of uniform and varying diameters. *J Appl Phys*. 2020;128(5):053103. doi:10.1063/5.0015650

83. Peoples J, Li X, Lv Y, Qiu J, Huang Z, Ruan X. A strategy of hierarchical particle sizes in nanoparticle composite for enhancing solar reflection. *Int J Heat Mass Transf*. 2019;131:487-494. doi:10.1016/j.ijheatmasstransfer.2018.11.059

84. Ma H, Wang L, Dou S, et al. Flexible Daytime Radiative Cooling Enhanced by Enabling Three-Phase Composites with Scattering Interfaces between Silica Microspheres and Hierarchical Porous Coatings. *ACS Appl Mater Interfaces*. 2021;13(16):19282-19290. doi:10.1021/acsami.1c02145

85. Zhu L, Raman A, Fan S. Color-preserving daytime radiative cooling. *Appl Phys Lett*. 2013;103(22):223902. doi:10.1063/1.4835995

86. Son S, Jeon S, Chae D, et al. Colored emitters with silica-embedded perovskite nanocrystals for efficient daytime radiative cooling. *Nano Energy*. 2021;79:105461. doi:10.1016/j.nanoen.2020.105461

87. Wang H, Yang Y, Wang L. Switchable wavelength-selective and diffuse metamaterial absorber/emitter with a phase transition spacer layer. *Appl Phys Lett*. 2014;105(7). doi:10.1063/1.4893616

88. Taylor S, Yang Y, Wang L. Vanadium dioxide based Fabry-Perot emitter for dynamic radiative cooling applications. *J Quant Spectrosc Radiat Transf*. 2017;197:76-83. doi:10.1016/j.jqsrt.2017.01.014

89. Ono M, Chen K, Li W, Fan S. Self-adaptive radiative cooling based on phase change materials. *Opt Express*. 2018;26(18):A777. doi:10.1364/oe.26.00a777

90. Xia Z, Fang Z, Zhang Z, Shi K, Meng Z, Meng Z. Easy Way to Achieve Self-Adaptive Cooling of Passive Radiative Materials. *ACS Appl Mater Interfaces*. 2020;12(24):27241-27248. doi:10.1021/acsami.0c05803

91. Taylor S, Long L, McBurney R, Sabbaghi P, Chao J, Wang L. Spectrally-selective vanadium dioxide based tunable metafilm emitter for dynamic radiative cooling. *Sol Energy Mater Sol Cells*. 2020;217:110739. doi:10.1016/j.solmat.2020.110739

92. Barker Jr A S, Verleur H W GHJ. Infrared optical properties of vanadium dioxide above and below the transition temperature. *Phys Rev Lett*. 1966;17(26):1286.

93. Hao Q, Li W, Xu H, et al. VO2/TiN Plasmonic Thermochromic Smart Coatings for Room-Temperature Applications. *Adv Mater*. 2018;30(10):1705421. doi:10.1002/adma.201705421

94. Mandal J, Jia M, Overvig A, et al. Porous Polymers with Switchable Optical Transmittance for Optical and Thermal Regulation. *Joule*. 2019;3(12):3088-3099. doi:10.1016/j.joule.2019.09.016

95. Sun S, Yang W, Zhang C, et al. Real-Time Tunable Colors from Microfluidic Reconfigurable All-Dielectric Metasurfaces. *ACS Nano*. 2018;12(3):2151-2159. doi:10.1021/acsnano.7b07121

96. Liu X, Tian Y, Chen F, Ghanekar A, Antezza M, Zheng Y. Continuously variable emission for mechanical deformation induced radiative cooling. *Commun Mater*. 2020;1(1):1-7. doi:10.1038/s43246-020-00098-8

97. Li X, Sun B, Sui C, et al. Integration of daytime radiative cooling and solar heating for year-round energy saving in buildings. *Nat Commun*. 2020;11(1):1-9. doi:10.1038/s41467-020-19790-x

98. Zhao D, Aili A, Yin X, Tan G, Yang R. Roof-integrated radiative air-cooling system to achieve cooler attic for building energy saving. *Energy Build*. 2019;203:109453. doi:10.1016/j.enbuild.2019.109453

99. Algarni S. Potential for cooling load reduction in residential buildings using cool roofs in the harsh climate of Saudi Arabia. *Energy Environ*. 2019;30(2):235-253. doi:10.1177/0958305X18787340

100. Torgerson E, Hellhake J. Polymer solar filter for enabling direct daytime radiative cooling. *Sol Energy Mater Sol Cells*. 2020;206:110319. doi:10.1016/j.solmat.2019.110319

101. Synnefa A, Santamouris M, Akbari H. Estimating the effect of using cool coatings on energy loads and thermal comfort in residential buildings in various climatic conditions. *Energy Build*. 2007;39(11):1167-1174. doi:10.1016/j.enbuild.2007.01.004

102. Fang H, Zhao D, Yuan J, et al. Performance evaluation of a metamaterial-based new cool roof using improved Roof Thermal Transfer Value model. *Appl Energy*. 2019;248:589-599. doi:10.1016/j.apenergy.2019.04.116

103. Xu T, Sathaye J, Akbari H, Garg V, Tetali S. Quantifying the direct benefits of cool roofs in an urban setting: Reduced cooling energy use and lowered greenhouse gas emissions. *Build Environ*. 2012;48(1):1-6. doi:10.1016/j.buildenv.2011.08.011

104. Akbari H, Matthews HD. Global cooling updates: Reflective roofs and pavements. *Energy Build*. 2012;55:2-6. doi:10.1016/j.enbuild.2012.02.055

105. Pisello AL, Castaldo VL, Pignatta G, Cotana F, Santamouris M. Experimental in-lab and in-field analysis of waterproof membranes for cool roof application and urban heat island mitigation. *Energy Build*. 2016;114:180-190. doi:10.1016/j.enbuild.2015.05.026

106. Yew MC, Ramli Sulong NH, Chong WT, Poh SC, Ang BC, Tan KH. Integration of thermal insulation coating and moving-air-cavity in a cool roof system for attic temperature reduction. *Energy Convers Manag*. 2013;75:241-248. doi:10.1016/j.enconman.2013.06.024

107. Testa J, Krarti M. A review of benefits and limitations of static and switchable cool roof systems. *Renew Sustain Energy Rev*. 2017;77:451-460. doi:10.1016/j.rser.2017.04.030

108. Guo R, Gao Y, Zhuang C, et al. Optimization of cool roof and night ventilation in office buildings: A case study in Xiamen, China. *Renew Energy*. 2020;147:2279-2294. doi:10.1016/j.renene.2019.10.032

109. Chen J, Lu L. Comprehensive evaluation of thermal and energy performance of radiative roof cooling in buildings. *J Build Eng*. 2021;33:101631. doi:10.1016/j.jobe.2020.101631

110. Zhang Z, Tong S, Yu H. Life Cycle Analysis of Cool Roof in Tropical Areas. *Procedia Eng*. 2016;169:392-399. doi:10.1016/j.proeng.2016.10.048

111. Akbari H, Matthews HD. Global cooling updates : Reflective roofs and pavements. *Energy Build*. 2012;55:2-6. doi:10.1016/j.enbuild.2012.02.055

112. Chen J, Lu L. Development of radiative cooling and its integration with buildings: A comprehensive review. *Sol Energy*. 2020;212:125-151. doi:10.1016/j.solener.2020.10.013

113. Goldstein EA, Raman AP, Fan S. Sub-ambient non-evaporative fluid cooling with the sky. *Nat Energy*. 2017;2:1-7. doi:10.1038/nenergy.2017.143

114. Hu M, Zhao B, Li J, Wang Y, Pei G. Preliminary thermal analysis of a combined photovoltaic e photothermic e nocturnal radiative cooling system. *Energy*. 2017;137:419-430. doi:10.1016/j.energy.2017.03.075

115. Miyawaki R, Satake A, Mitani Y, Ushifusa Y. Consideration of reducing purchased power using photovoltaic excess power by thermal radiative cooling / heating system. *Energy Reports*. 2020;6:814-821. doi:10.1016/j.egyr.2020.11.127

116. Farmahini M, Heidarinejad G, Delfani S. A two-stage system of nocturnal radiative and indirect evaporative cooling for conditions in Tehran. *Energy Build*. 2010;42(11):2131-2138. doi:10.1016/j.enbuild.2010.07.003

117. Jeong SY, Tso CY, Zouagui M, Wong YM, Chao CYH. A numerical study of daytime passive radiative coolers for space cooling in buildings. *Build Simul*. 2018;11(5):1011-1028. doi:10.1007/s12273-018-0474-4

118. Zhao D, Yin X, Xu J, Tan G, Yang R. Radiative sky cooling-assisted thermoelectric cooling system for building applications. *Energy*. 2020;190:116322. doi:10.1016/j.energy.2019.116322

119. Yuan J, Yin H, Cao P, Yuan D, Xu S. Energy for Sustainable Development Daytime radiative cooling of enclosed water using spectral selective metamaterial based cooling surfaces. *Energy Sustain Dev*. 2020;57:22-31. doi:10.1016/j.esd.2020.04.008

120. Zhang K, Zhao D, Yin X, Yang R, Tan G. Energy saving and economic analysis of a new hybrid radiative cooling system for single-family houses in the USA. *Appl Energy*. 2018;224:371-381. doi:10.1016/j.apenergy.2018.04.115

121. Katramiz E, Al Jebaei H, Alotaibi S, Chakroun W, Ghaddar N, Ghali K. Sustainable cooling system for Kuwait hot climate combining diurnal radiative cooling and indirect evaporative cooling system. *Energy*. 2020;213:119045. doi:10.1016/j.energy.2020.119045

122. Spanaki A, Kolokotsa D, Tsoutsos T, Zacharopoulos I. Theoretical and experimental analysis of a novel low emissivity water pond in summer. *Sol Energy*. 2012;86(11):3331-3344. doi:10.1016/j.solener.2012.08.017

123. Tevar JAF, Castaño S, Marijuán AG, Heras MR, Pistono J. Modelling and experimental analysis of three radioconvective panels for night cooling. *Energy Build*. 2015;107:37-48. doi:10.1016/j.enbuild.2015.07.027

124. Liu Z, Tan H, Ma G. Experimental investigation on night sky radiant cooling performance of duct-type heat exchanger. *Int J Vent*. 2017;16(3):255-267. doi:10.1080/14733315.2017.1299520

125. Royne A, Dey CJ, Mills DR. Cooling of photovoltaic cells under concentrated illumination: A critical review. *Sol Energy Mater Sol Cells*. 2005;86(4):451-483. doi:10.1016/j.solmat.2004.09.003

126. Skoplaki E, Palyvos JA. On the temperature dependence of photovoltaic module electrical performance : A review of efficiency / power correlations. *Sol Energy*. 2009;83(5):614-624. doi:10.1016/j.solener.2008.10.008

127. Zhu L, Raman A, Wang KX, Anoma MA, Fan S. Radiative cooling of solar cells. *Optica*. 2014;1(1):32. doi:10.1364/optica.1.000032

128. Li W, Shi Y, Chen K, Zhu L, Fan S. A Comprehensive Photonic Approach for Solar Cell Cooling. *ACS Photonics*. 2017;4(4):774-782. doi:10.1021/acsphotonics.7b00089

129. Riverola A, Mellor A, Alonso Alvarez D, et al. Mid-infrared emissivity of crystalline silicon solar cells. *Sol Energy Mater Sol Cells*. 2018;174:607-615. doi:10.1016/j.solmat.2017.10.002

130. Huang Y, Pu M, Gao P, et al. Ultra-broadband large-scale infrared perfect absorber with optical transparency. *Appl Phys Express*. 2017;10(11):112601. doi:10.7567/APEX.10.112601

131. Safi TS, Munday JN. Improving photovoltaic performance through radiative cooling in both terrestrial and extraterrestrial environments. *Opt Express*. 2015;23(19):A1120. doi:10.1364/oe.23.0a1120

132. Wang Z, Kortge D, Zhu J, et al. Lightweight, Passive Radiative Cooling to Enhance Concentrating Photovoltaics. *Joule*. 2020;4(12):2702-2717. doi:10.1016/j.joule.2020.10.004

133. Lee A, Moon MW, Lim H, Kim WD, Kim HY. Water harvest via dewing. *Langmuir*. 2012;28(27):10183-10191. doi:10.1021/la3013987

134. Khalil B, Adamowski J, Shabbir A, et al. A review: dew water collection from radiative passive collectors to recent developments of active collectors. *Sustain Water Resour Manag*. 2016;2(1):71-86. doi:10.1007/s40899-015-0038-z

135. Zhou M, Song H, Xu X, et al. Vapor condensation with daytime radiative cooling. *Proc Natl Acad Sci U S A*. 2021;118(14):e2019292118. doi:10.1073/pnas.2019292118

136. Benlattar M, Laatioui S, Oualim EM, Mazroui M, Mouhsen A, Harmouchi M. Numerical modelling of lawsonite thin film as radiative cooling minerals for dew harvesting. *Results Phys*. 2017;7:1959-1964. doi:10.1016/j.rinp.2017.05.024

137. Maestre-Valero JF, Martin-Gorriz B, Martínez-Alvarez V. Dew condensation on different natural and artificial passive surfaces in a semiarid climate. *J Arid Environ*. 2015;116:63-70. doi:10.1016/j.jaridenv.2015.02.002

138. Al-Khayat O, Hong JK, Beck DM, Minett AI, Neto C. Patterned Polymer Coatings Increase the Efficiency of Dew Harvesting. *ACS Appl Mater Interfaces*. 2017;9(15):13676-13684. doi:10.1021/acsami.6b16248

139. Guan H, Sebben M, Bennett J. Radiative- and artificial-cooling enhanced dew collection in a coastal area of South Australia. *Urban Water J*. 2014;11(3):175-184. doi:10.1080/1573062X.2013.765494

140. Liu C, Fan J, Bao H. Hydrophilic radiative cooler for direct water condensation in humid weather. *Sol Energy Mater Sol Cells*. 2020;216:110700. doi:10.1016/j.solmat.2020.110700

141. Dong M, Zhang Z, Shi Y, Zhao X, Fan S, Chen Z. Fundamental Limits of the Dew-Harvesting Technology. *Nanoscale Microscale Thermophys Eng*. 2020;24(1):43-52. doi:10.1080/15567265.2020.1722300

142. Dai X, Sun N, Nielsen SO, et al. Hydrophilic directional slippery rough surfaces for water harvesting. *Sci Adv*. 2018;4(3):eaaq0919. doi:10.1126/sciadv.aaq0919

143. Chen M, Yan H, Zhou P, Chen XY. Performance analysis of solar thermophotovoltaic system with selective absorber/emitter. *J Quant Spectrosc Radiat Transf*. 2020;253:788-798. doi:10.1016/j.jqsrt.2020.107163

144. Chen M, Chen X, Yan H, Zhou P. Theoretical design of nanoparticle-based spectrally emitter for thermophotovoltaic applications. *Phys E Low-Dimensional Syst Nanostructures*. 2021;126:114471. doi:10.1016/j.physe.2020.114471

145. Raman AP, Li W, Fan S. Generating Light from Darkness. *Joule*. 2019;3(11):2679-2686. doi:10.1016/j.joule.2019.08.009

146. Fan L, Li W, Jin W, Orenstein M, Fan S. Maximal nighttime electrical power generation via optimal radiative cooling. *Opt Express*. 2020;28(17):25460. doi:10.1364/oe.397714

147. Ishii S, Dao TD, Nagao T. Radiative cooling for continuous thermoelectric power generation in day and night. *Appl Phys Lett*. 2020;117(1):013901. doi:10.1063/5.0010190

148. Zhang K, Zhao D, Zhai Y, Yin X, Yang R, Tan G. Modelling study of the low-pump-power demand constructal T-shaped pipe network for a large scale radiative cooled-cold storage system. *Appl Therm Eng*. 2017;127:1564-1573. doi:10.1016/j.applthermaleng.2017.08.131

149. Hsu PC, Song AY, Catrysse PB, et al. Radiative human body cooling by nanoporous polyethylene textile. *Science (80-)*. 2016;353(6303):1019-1023. doi:10.1126/science.aaf5471

150. Zeng S, Pian S, Su M, Liu X, Wu M, Chen M. Hierarchical-morphology metafabric for scalable passive daytime radiative cooling. *Science (80-)*. 2021;5484:1-9.

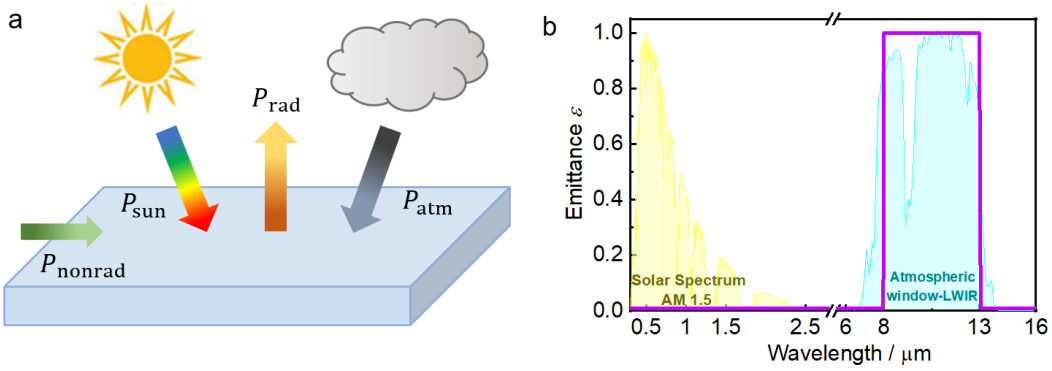

Figure 1. Fundamentals of PDRC. (a) Schematic diagram and heat transfer processes of PDRC coatings. P_{atm} and P_{sun} are the absorbed powers from the atmospheric and solar irradiations, respectively. P_{rad} is the thermal radiation power of the PDRC coating. P_{nonrad} denotes the nonradiative heat transfer processes (convection and conduction) between the coating and ambient environment. (b) Normalized solar spectral intensity and LWIR atmospheric transparent window represented by the yellow and green curves, respectively. Ideal spectrum of the PDRC coating is represented within the purple box

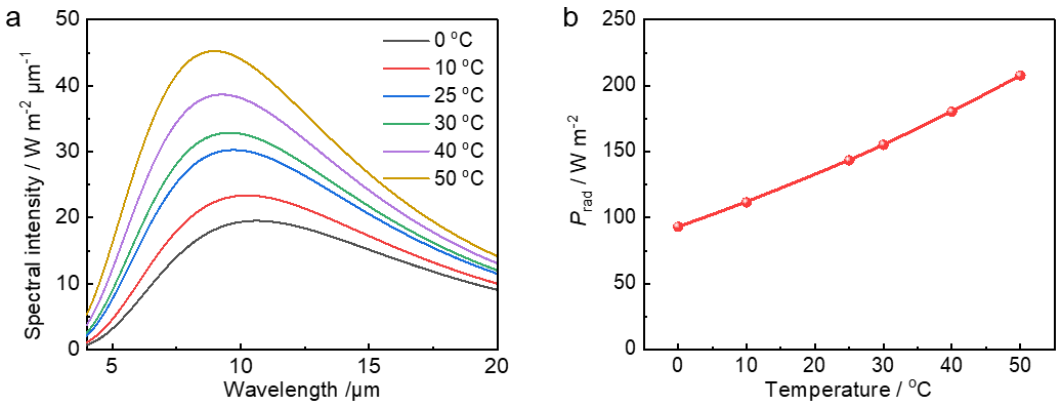

Figure 2. Radiative power of the PDRC coating at different temperatures. (a) Blackbody spectral radiative powers at different temperatures. (b) Radiative power P_{rad} of an ideal PDRC coating at different temperatures through the ideal atmospheric LWIR window.

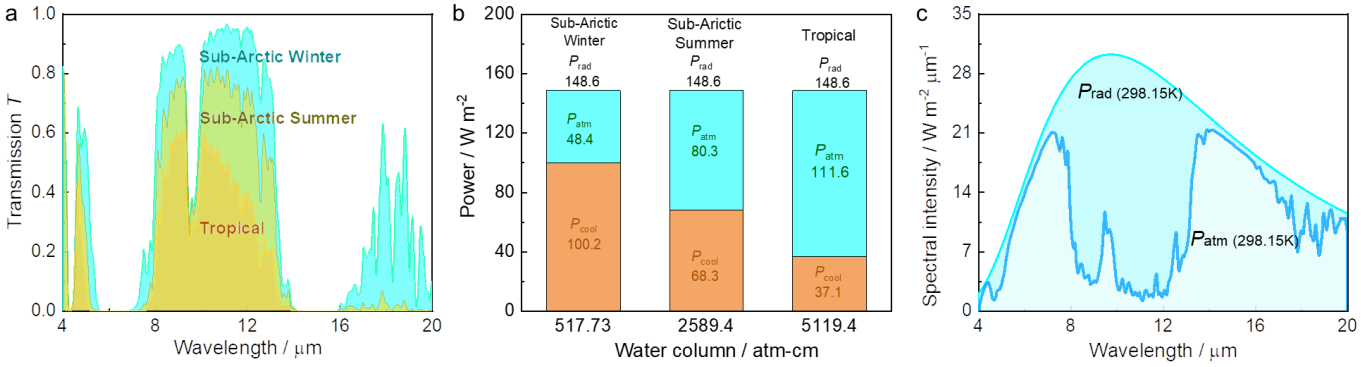

Figure 3 Absorbed power from atmospheric irradiation. (a) Atmospheric transmittance under Sub-Arctic Winter (water column = 517.7 atm-cm and visibility = 23.0 km), Sub-Arctic Summer (water column = 2589.4 atm-cm and visibility = 23.0 km) and Tropical (water column = 5119.4 atm-cm and visibility = 23.0 km) conditions. The atmospheric transmittance data is obtained from MODTRAN. (b) Nighttime cooling and absorbed atmospheric irradiation powers of an ideal radiative coating at different water columns. (c) Spectral power densities $P_{\mathrm{rad}}(\lambda)$ and $P_{\mathrm{atm}}(\lambda)$ at the ambient temperature T_{atm} = 298.15 K, and the temperature of coating is 298.15 K.

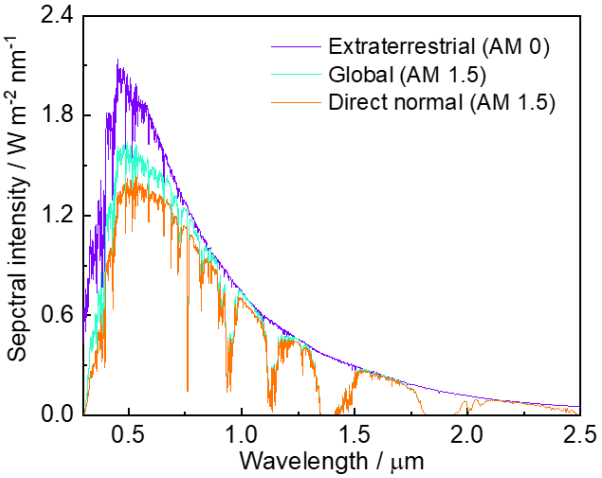

Figure 4 Solar spectral irradiance of the extraterrestrial (AM 0), global tilted (AM 1.5), and direct normal spectra (AM 1.5). The AM 1.5 standard spectrum refers to exactly two standard terrestrial solar spectral irradiance spectra. The two spectra define a standard direct normal spectral irradiance and a standard total spectral irradiance. The direct normal spectrum is the direct component that contributes to the total global (hemispherical) spectrum.

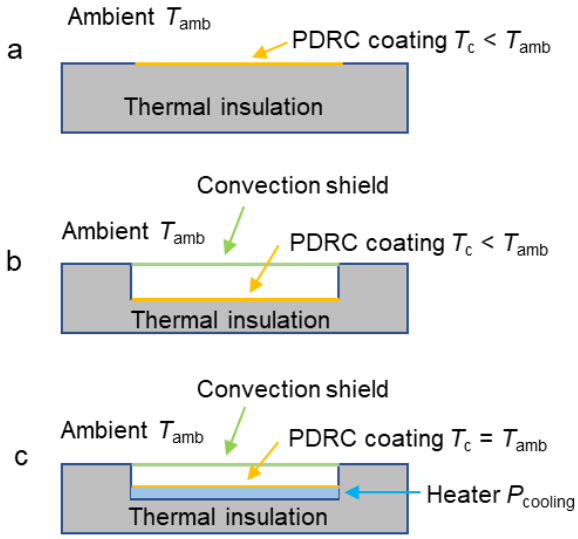

Figure 5 Schematic diagrams of three different devices for PDRC coatings. (a) The PDRC coating is placed on a substrate and is directly exposed to the ambient atmosphere ($T_c < T_{amb}$). (b) The PDRC coating is placed in a well-insulated enclosure and a convection shield is employed at the top to suppress the thermal losses caused by convection and conduction heat transfer at sub-ambient conditions ($T_c < T_{amb}$). (c) Instead of demonstrating a temperature difference between the radiative cooling surface and ambient temperatures ($T_c - T_{amb}$), the PDRC coating is placed on a heater to maintain $T_c = T_{amb}$ for measuring the net cooling power.

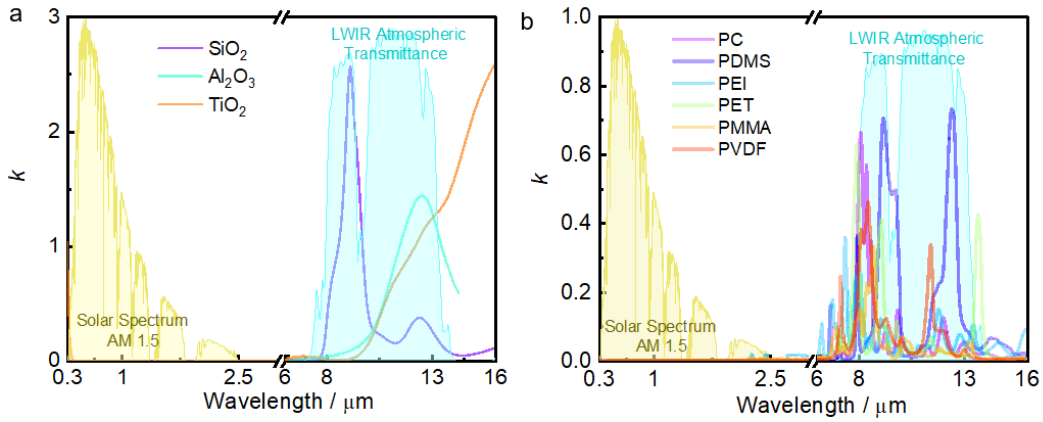

Figure 6 Complex refractive indices for (a) inorganic materials (Reproduced with permission: Copyright 2007 and 2012, OSA)[62,63], (Reproduced with permission: Copyright 2016, Wiley)[64], and (b) organic polymers used for PDRC (Reproduced with permission: Copyright 2018, AAAS) [15], (Reproduced with permission: Copyright 2020, Elsevier) [65].

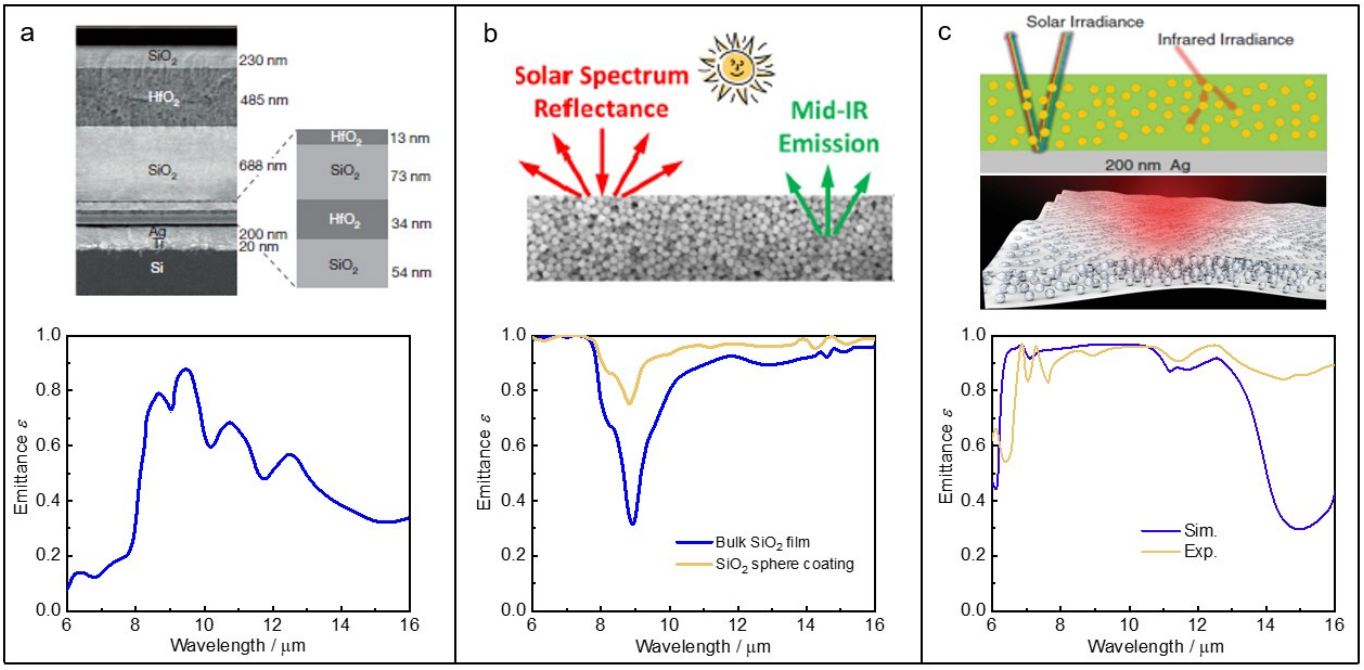

Figure 7 Mid-infrared emittance of inorganic materials based on (a) multi-layer coating (Reproduced with permission: Copyright 2014, Spring Nature)[4], (b) microsphere stacked coating (Reproduced with permission: Copyright 2018, ACS)[20], (Reproduced with permission: Copyright 2021, Elsevier)[67], and (c) inorganic microsphere mixed with the organic polymer (Reproduced with permission: Copyright 2017, AAAS)[18].

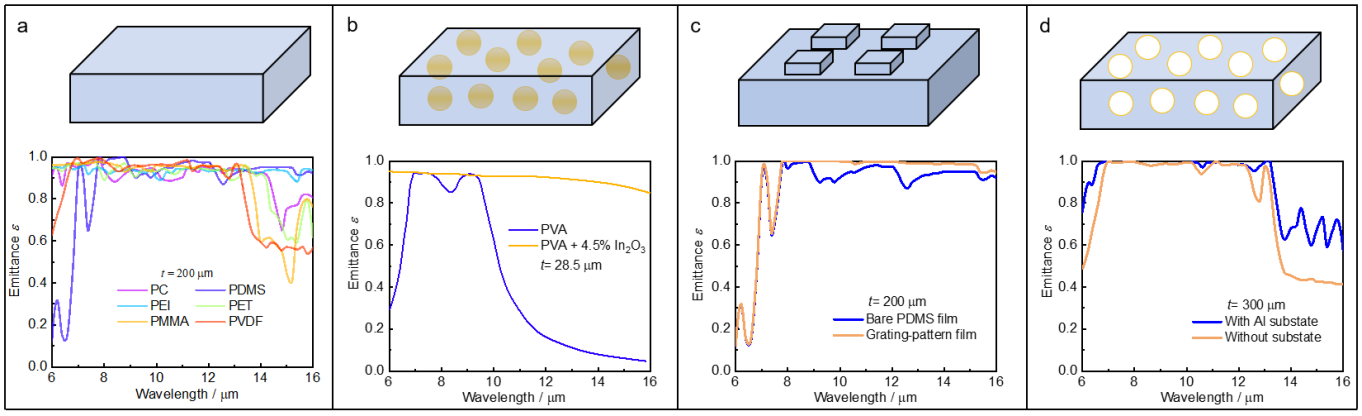

Figure 8 Mid-infrared emittance of organic polymers based on (a) bulk film coating (Reproduced with permission: Copyright 2019, Elsevier)[33], (Reproduced with permission: Copyright 2021, IPO Science)[68], (b) plasmonic microsphere coating (Reproduced with permission: Copyright 2020, ACS)[35], (c) surface microstructure coating (Reproduced with permission: Copyright 2020, AIP)[30], (Reproduced with permission: Copyright 2020, IPO Science)[68], and (d) porous polymer coating (Reproduced with permission: Copyright 2021, ACS)[59].

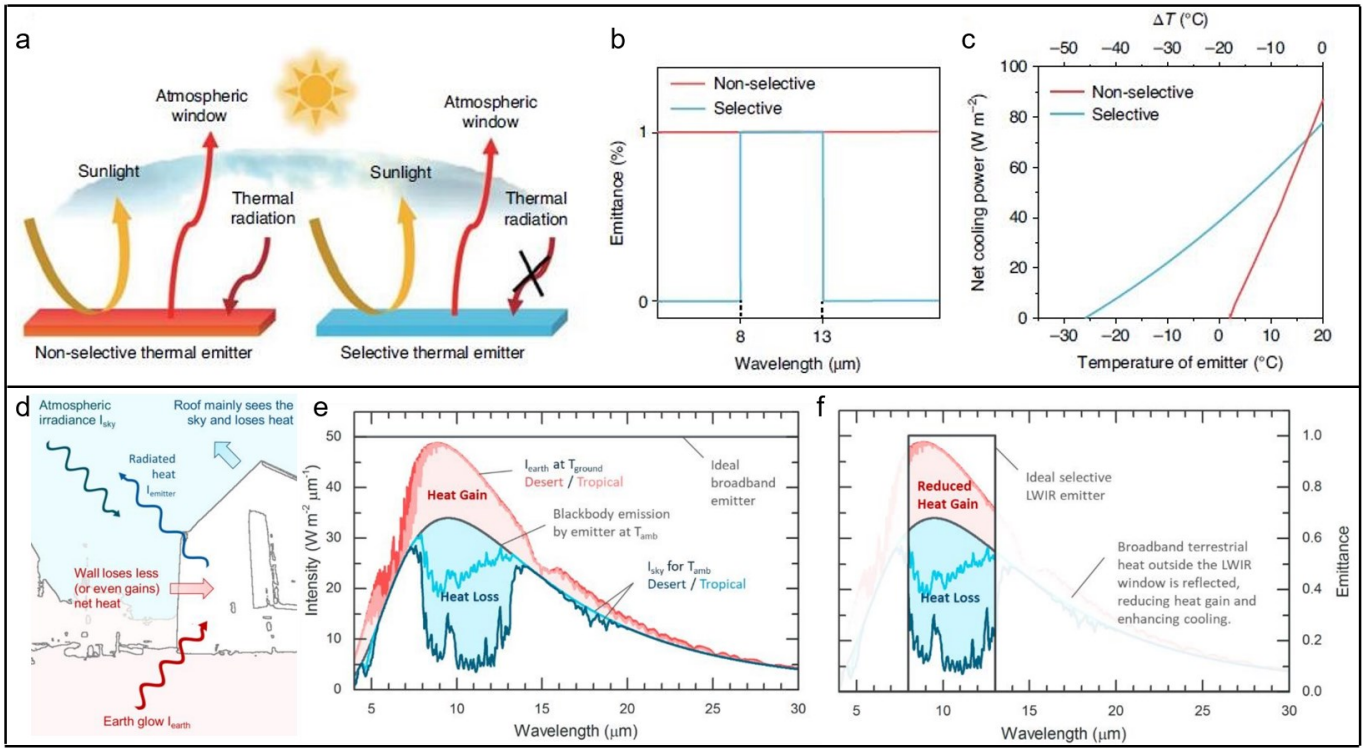

Figure 9 Theoretical analysis of a selective thermal emitter in the mid-infrared region. (a)–(c) Horizontal coating facing the sky (Reproduced with permission: Copyright 2021, Spring Nature)[77]: (a) Schematic of the radiative heat transfer process of the selective and non-selective thermal emitters. The selective thermal emitter has a more suppressed absorption of thermal radiation from the surroundings as compared to that of the non-selective emitter. (b) The mid-infrared spectrum of an ideal selective thermal emitter (blue line) and a non-selective thermal emitter (red line). (c) Net cooling power as a function of the emitter temperature based on a typical atmospheric transmittance and without non-radiation heat transfer. (d)–(e) Vertically oriented coating [34]: (d) Schematic showing the possible radiative heat transfer between a vertical wall and the ground and sky in its view. (e) The possible heat gain (red) from the ground (at 55 °C) and heat loss (blue) to the sky, as shown for an ideal broadband emitter at ambient temperature (here 32 °C) under desert (TPW 10.5 mm) and tropical (TPW 58.6 mm) climates. (f) Analog for an ideal selective LWIR emitter. By reflecting thermal radiation outside the

window, the selective emitter filters out most of the broadband thermal radiation from the ground and facilitates better cooling when the ground in view is hot.

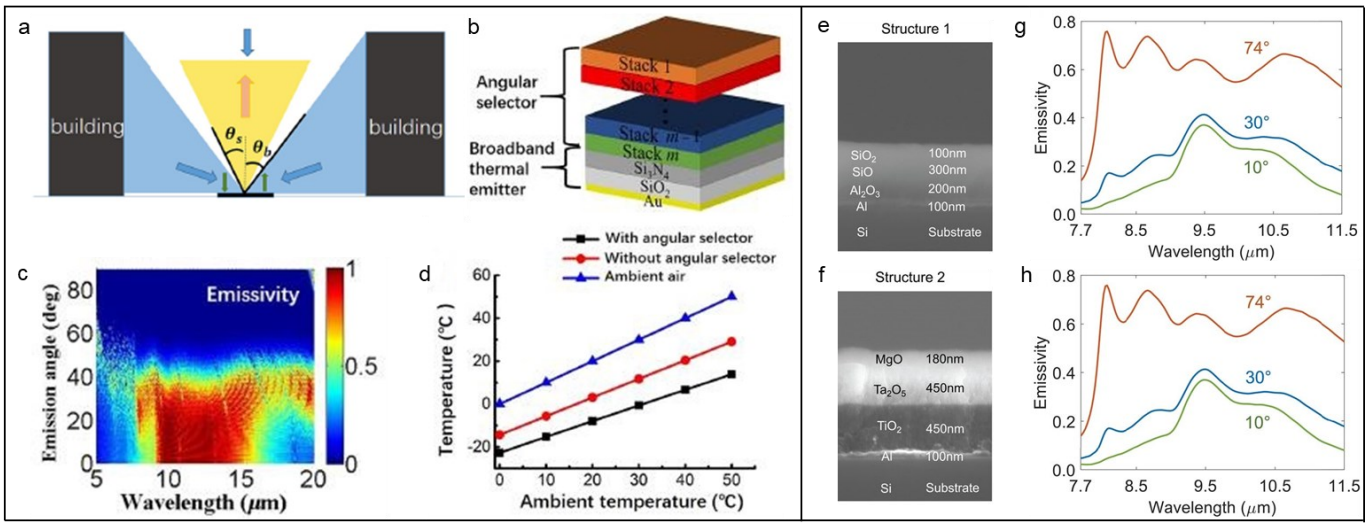

Figure 10 Directional thermal emitter used in PDRC. (a)–(d) Directional emitter based on angular selector (Reproduced with permission: Copyright 2020, APS)[78]: (a) Radiative cooling with angular control of thermal emission when there are surrounding buildings. (b) Directional emitter consisting of a broadband thermal emitter at the bottom and a multilayer angular selector on the top. (c) Spectral emittance of the directional emitter. (d) Equilibrium temperatures of ambient air (blue line), broadband thermal emitter (red line), and emitter (black line) for different ambient temperatures. The effective heat transfer coefficient h = 0.5 W m^{-2} K^{-1}. (e)–(i) Directional emitter based on gradient epsilon-near-zero material structures (Reproduced with permission: Copyright 2021, AAAS)[79]. (e) and (f) SEM images of the experimentally fabricated multilayer photonic film structures. (g) and (h) Measured emittance of the two photonic structures at varying wavelengths at three different angles for p-polarization. Both the photonic structures exhibit a strong contrast between emissive and reflective states as a function of angle of incidence.

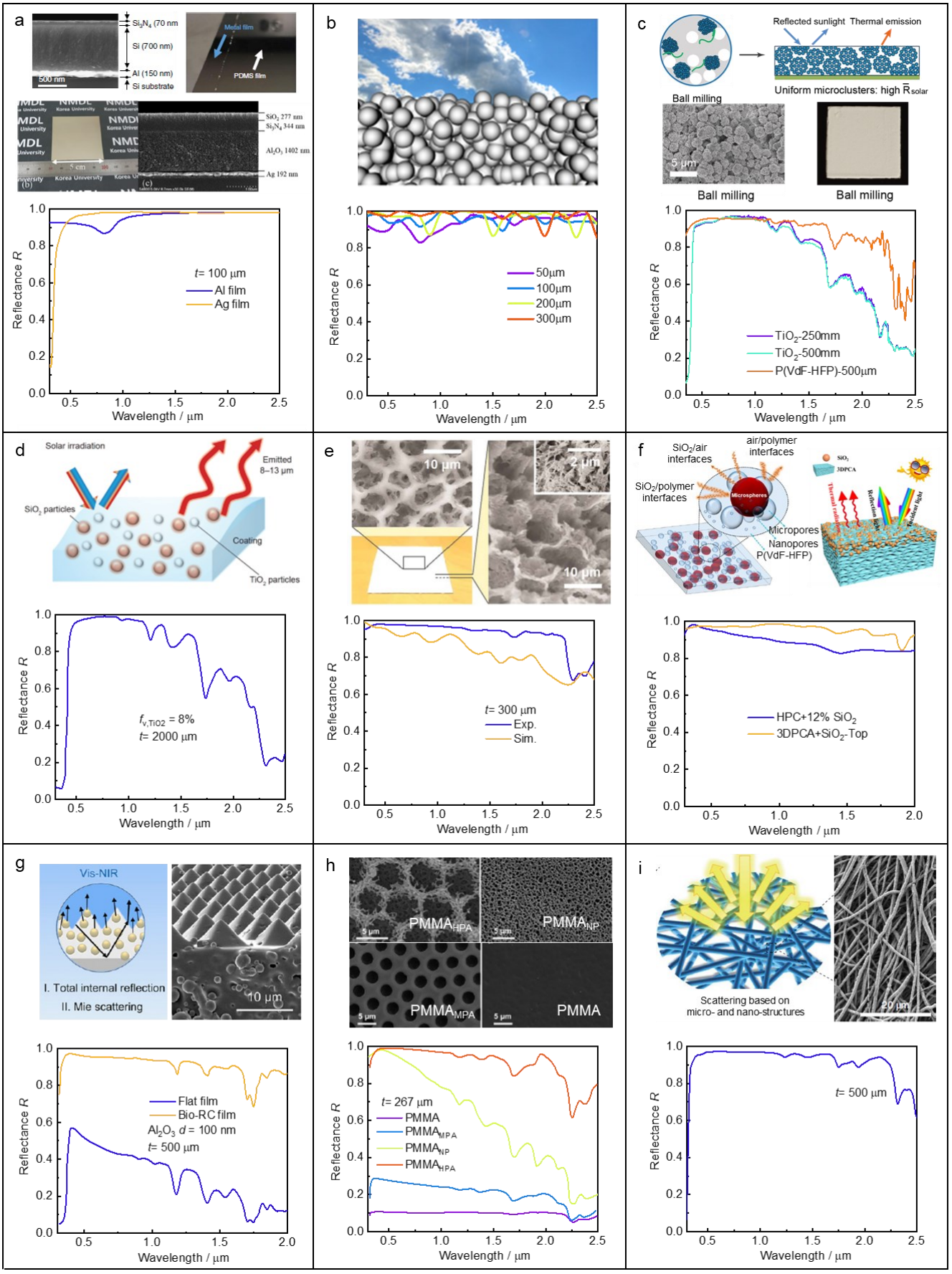
a
Si3N4 (70 nm)
Si (700 nm)
Al (150 nm)
Si substrate
500 nm
Metal film
PDMS film
SiO2 277 nm
Si3N4 344 nm
Al2O3 1402 nm
Ag 192 nm
Reflectance R
Wavelength / μm
t= 100 μm
Al film
Ag film
b
50μm
100μm
200μm
300μm
c
Reflected sunlight
Thermal emission
Uniform microclusters: high R̄solar
Ball milling
5 μm
Ball milling
Ball milling
TiO2-250mm
TiO2-500mm
P(VdF-HFP)-500μm
d
Solar irradiation
Emitted 8–13 μm
SiO2 particles
Coating
TiO2 particles
fv,TiO2 = 8%
t= 2000 μm
e
10 μm
2 μm
10 μm
t= 300 μm
Exp.
Sim.
f
SiO2/air interfaces
air/polymer interfaces
SiO2/polymer interfaces
Microspheres
Micropores
Nanopores
P(VdF-HFP)
HPC+12% SiO2
3DPCA+SiO2-Top
g
Vis-NIR
I. Total internal reflection
II. Mie scattering
10 μm
Flat film
Bio-RC film
Al2O3 d = 100 nm
t= 500 μm
h
PMMAHPA
PMMANP
PMMAMPA
PMMA
5 μm
t= 267 μm
PMMA
PMMAMPA
PMMANP
PMMAHPA
i
Scattering based on
micro- and nano-structures
20 μm
t= 500 μm

Figure 11 General strategies to reflect solar irradiation. (a) Metal reflector (such as: Ag and Al) (Reproduced with permission: Copyright 2019, Spring Nature)[32], and (Reproduced with permission: Copyright 2021, ACS)[51]. (b) Inorganic dielectric microsphere random coating (such as: TiO_2, SiO_2, and Al_2O_3 microspheres) (Reproduced with permission: Copyright 2018, ACS)[20], and (Reproduced with permission: Copyright 2021, Elsevier)[67]. (c) Organic polymer microsphere coating (such as: P(VdF-HFP)) (Reproduced with permission: Copyright 2021, Wiley)[70]. (d) Polymer microsphere coating (Reproduced with permission: Copyright 2021 and 2019, Elsevier)[21,83], and (Reproduced with permission: Copyright 2021, Spring)[46]. (e) Porous polymer coating (such as: P(VdF-HFP), PDMS, and PMMA) (Reproduced with permission: Copyright 2018, AAAS)[15], and (Reproduced with permission: Copyright 2021, ACS)[59]. (f) Porous polymer coating with dielectric microspheres (Reproduced with permission: Copyright 2021, Elsevier)[55], and (Reproduced with permission: Copyright 2021, ACS)[84]. (g) Polymer microsphere coating modified by the surface microstructure (Reproduced with permission: Copyright 2020, PNAS)[44]. (h) Porous polymer coating modified by the surface microstructure (Reproduced with permission: Copyright 2021, Spring Nature)[31]. (i) Textile reflector based on the polymer (such as: PEO) (Reproduced with permission: Copyright 2021, Spring Nature)[77].

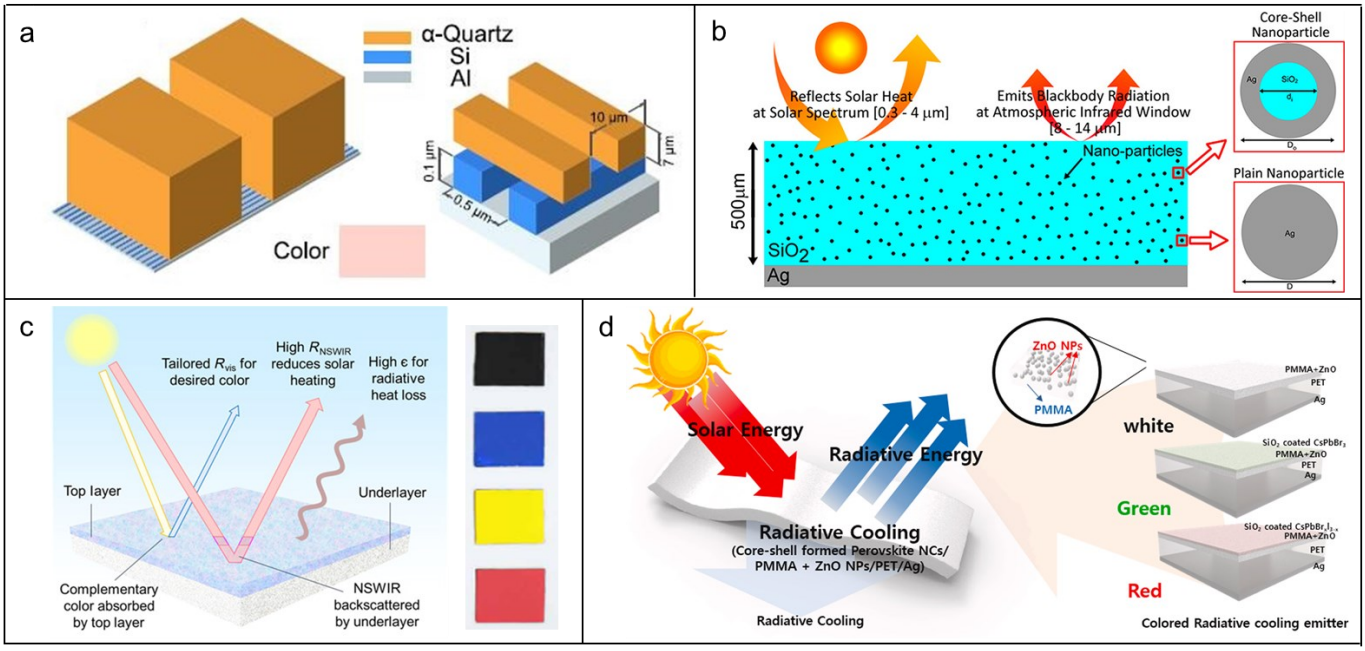

Figure 12 Strategies for colored PDRC coatings: (a) Schematic of the color-preserving structure based on the structural color of the dielectric structure, with quartz bar array on top of the original structure of silicon nanowires (Reproduced with permission: Copyright 2013, AIP).[85] (b) Schematic of the colored coating based on the structural color of the plasmonic structure, consisting of a silver reflector and Ag@SiO_2 nanoparticles embedded in silica (Reproduced with permission: Copyright 2020, ACS).[49] (c) Schematic illustrating the interaction between sunlight and thermal radiation with the paintable bilayer design. a selective reflection in the visible spectrum yields dye color (Reproduced with permission: Copyright 2020, AAAS). [22] (d) Schematic of colored emitter for daytime radiative cooling devices with silica-embedded perovskite nanocrystals (Reproduced with permission: Copyright 2021, Elsevier). [86]

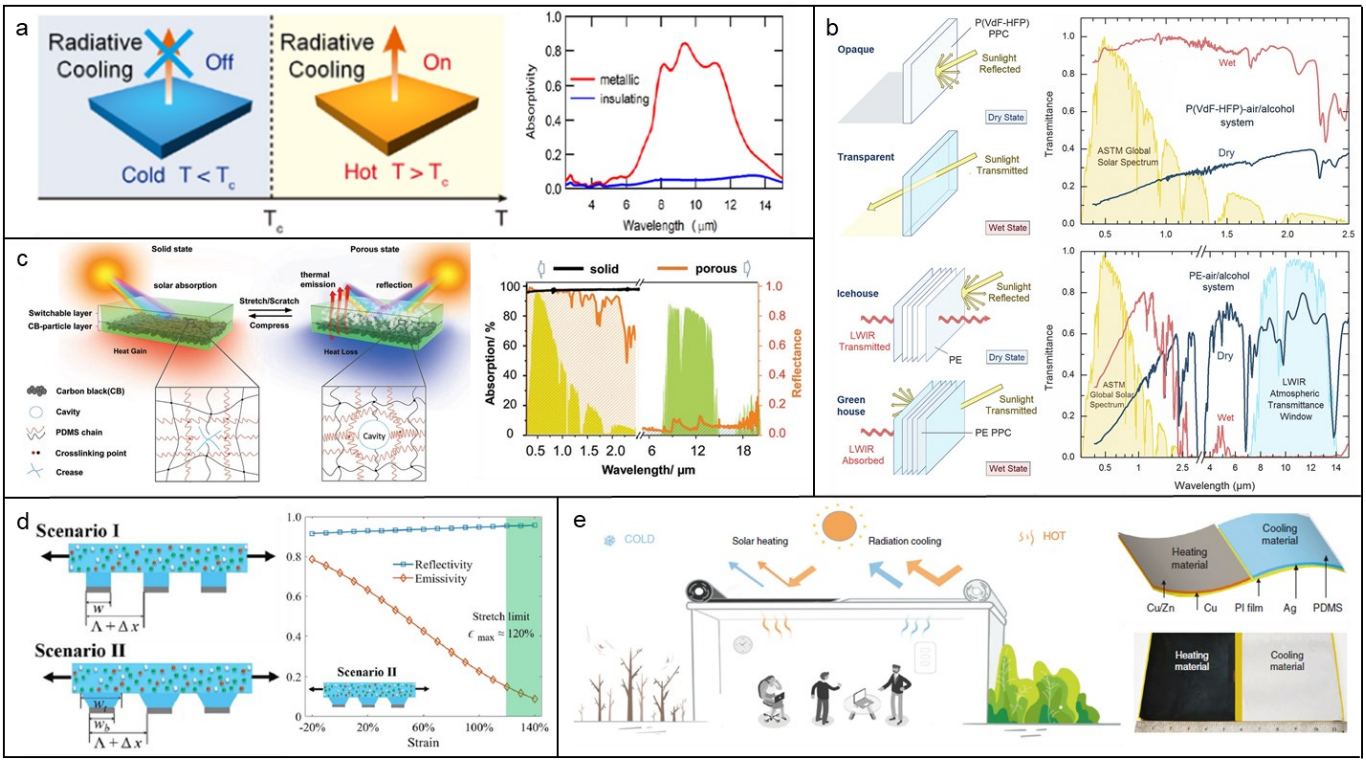

Figure 13 Dynamic switchable coatings for thermal management. (a) Temperature-dependent coatings: schematic of self-adaptive radiative cooling coating consisting of $VO_2/MgF_2/W$ tri-layer and a spectrally-selective filter, and its angle and polarization averaged absorptivity spectrum of the bottom radiative cooler in presence of the top filter (Reproduced with permission: Copyright 2018, OSA)[89]. (b) Dielectric environment dependent coatings: optical Switching of porous polymer coatings as exemplified by P(VdF-HFP) switching white to transparent ($\Delta T_{solar} = 0.74$) and PE switching icehouse to greenhouse ($\Delta T_{solar} = 0.33$ and $\Delta T_{LWIR} = 0.64$) by wetting and drying (Reproduced with permission: Copyright 2019, Cell)[94]. (c)–(e) mechanical force dependent coatings: (c) Schematic of the bilayer structure consisting of a switchable PDMS top layer and carbon black particle-embedded bottom layer and typical spectral properties of the switchable coating (Reproduced with permission: Copyright 2020, Wiley)[50]. (d) Schematic of a switchable coating consisting of PDMS and Ag film under stretching or compression due to the mechanical strain, and $\bar{R}_{solar}$, $\bar{\varepsilon}_{LWIR}$ changing with different strains (Reproduced with permission: Copyright 2020, Spring Nature)[96]. (f) Schematic

of the dual-mode device at heating (left) and cooling (right) mode consisting of dual-mode heating (Cu/Zn solar selective absorber) / cooling (PDMS/Ag cooler) material (Reproduced with permission: Copyright 2020, Spring Nature)[97].

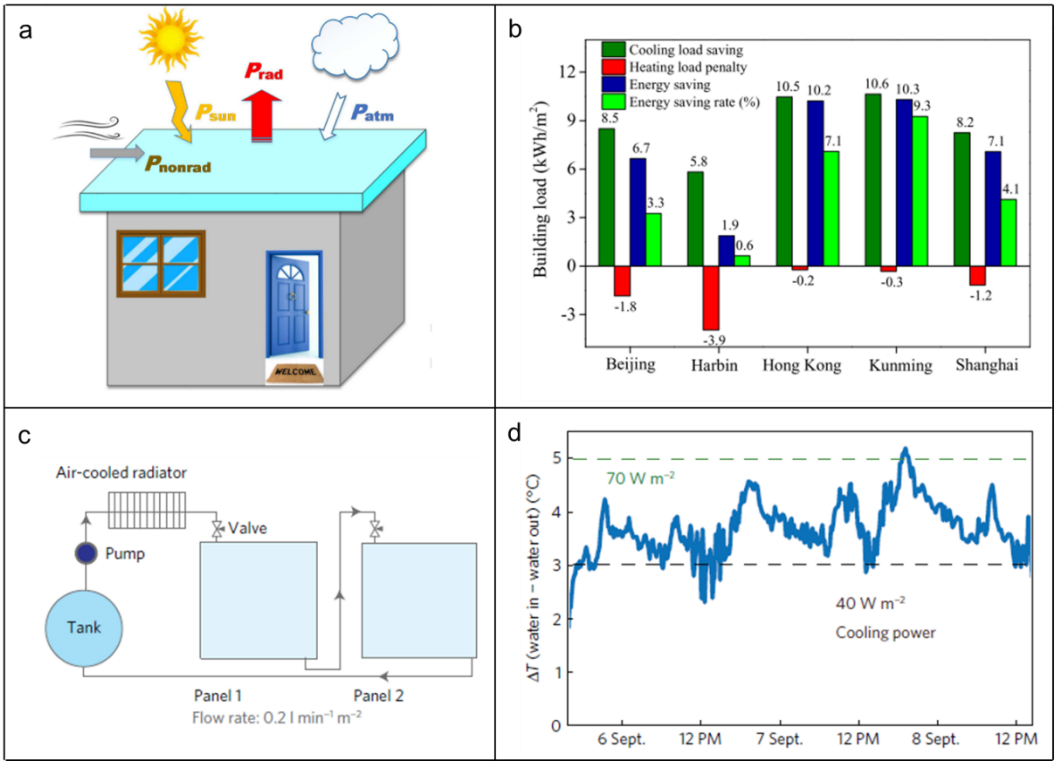

Figure 14 PDRC for space cooling: (a) Energy flows through a radiative roof surface. (b) Annual building energy consumptions and savings in five typical cities: Beijing, Harbin, Hong Kong, Kunming, and Shanghai (Reproduced with permission: Copyright 2021, Elsevier)[109]. (c) A schematic of the piping configuration in the test set-up, highlighting the presence of an air-cooled radiator (to bring the fluid inlet to the panels to the ambient air temperature), pump and tank. (d) Three days of data showing the temperature difference between the outlet and inlet of the two panels at a flow rate of 0.2 L min^{-1} m^{-2} (Reproduced with permission: Copyright 2017, Spring Nature)[113].

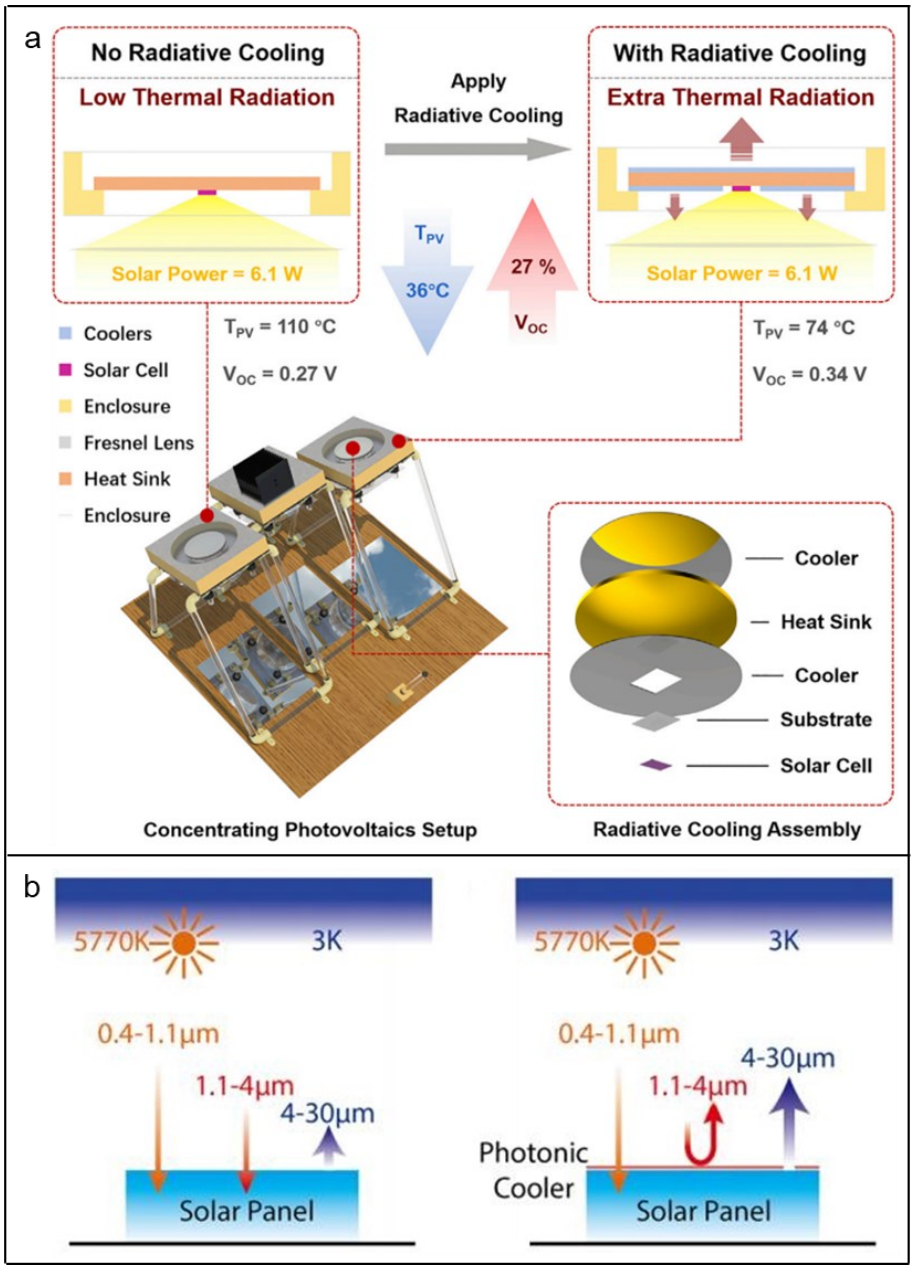

Figure 15 PDRC for solar cell cooling: (a) Experimental concentrating photovoltaics setup by applying the cheap, passive, and lightweight PDRC coating on top of the traditional cooling approaches (Reproduced with permission: Copyright 2020, Cell)[132]. (b) Schematic of the solar absorption and thermal radiation properties of existing solar panels with or without cooler. Suboptimal radiative cooling and strong parasitic sub-band-gap absorption are observed in existing solar panels. With a photonic cooler coated on top of solar panel, the radiative cooling

can be improved and the sub-band-gap solar radiation can be strongly reflected (Reproduced with permission: Copyright 2017, ACS)[128].

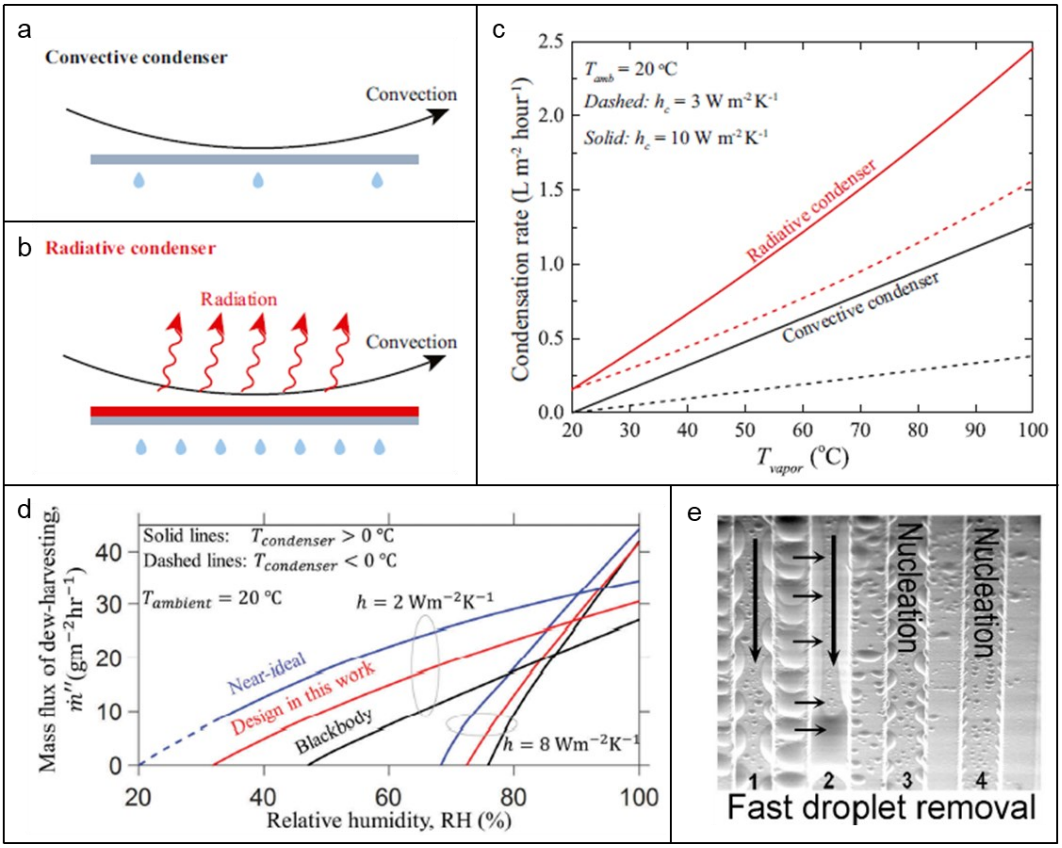

Figure 16 PDRC for water harvesting from atmosphere: (a) to (c) Performances of convective condenser and radiative condenser: (a) and (b) Schematic of a convective condenser (a) and our radiative condenser (b). The convective condenser dissipates heat through only convection, while the radiative condenser dissipates heat through both convection and radiation. (c) Theoretically calculated condensation rates of the convective (black) and radiative condenser (red), assuming an ambient temperature of 20 °C. To analyze the theoretical upper bound of condensation rate, we assume a relative humidity of 100% throughout our calculation. (Reproduced with permission: Copyright 2021, PNAS)[135] (d) Relative humidity dependence of the mass flux of dew-harvesting for three different emitters under two representative scenarios: h = 2 W m^{-2} K^{-1} and 8 W m^{-2} K^{-1}. The near-ideal emitter (blue) surpasses its blackbody counterpart (black) in both scenarios. (Reproduced with permission: Copyright 2020, Taylor & Francis)[141]. (e) Condensation on a hydrophilic directional slippery, rough surface. Smaller

droplets move into the slippery microchannels, and larger droplets can be effectively drained away by the slippery microchannels. (Reproduced with permission: Copyright 2018, AAAS)[142].

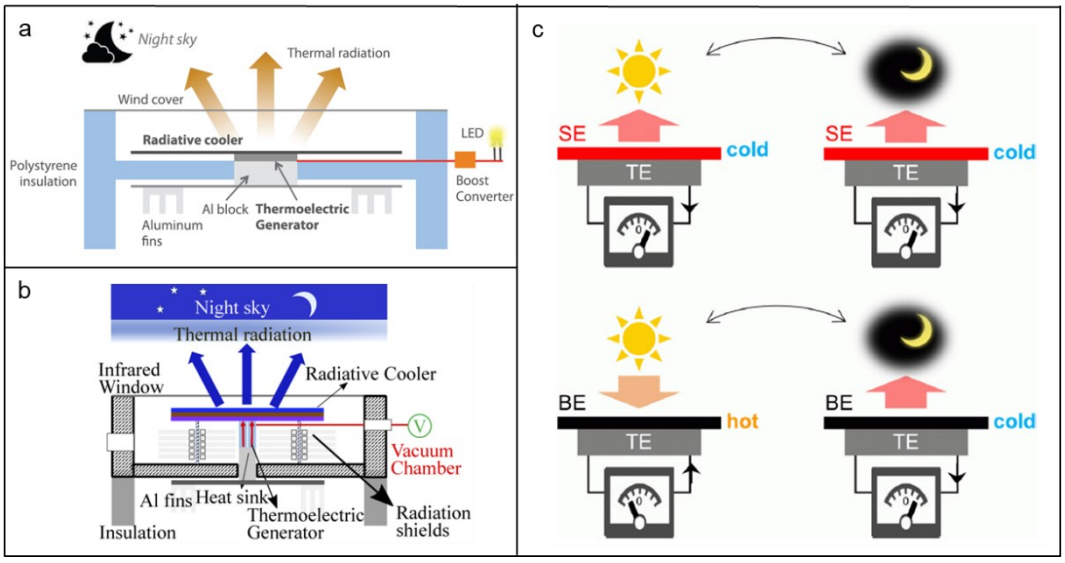

Figure 17 Radiative cooling for electricity generation. (a) Schematic of the low-cost night-time TE generator device and its key components (Reproduced with permission: Copyright 2019, Cell)[145]. (b) Proposed system for optimal power generation at nighttime (Reproduced with permission: Copyright 2020, OAS)[146]. (c) Conceptual drawing of TE devices having a wavelength selective emitter (SE) and a broadband emitter (BE) on the top. When an SE is on the top, the top temperature is always cooler than the bottom, and the sign of the TE voltage does not change; however, when a BE is on the top, the top is hotter and cooler than the bottom in daytime and nighttime, respectively. Thus, the generated TE voltage changes its sign. (Reproduced with permission: Copyright 2020, AIP)[147]

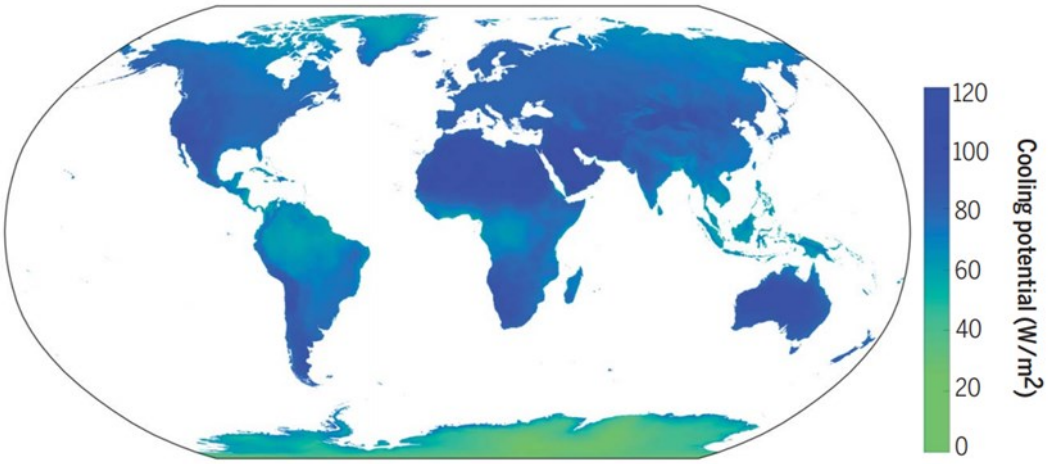

Figure 18 Global radiative cooling potential based on the global meteorological datasets collected between 2015 and 2019, including rainy and cloudy weather conditions. It uses an ideal wavelength-selective radiative cooling material with 5% solar absorbance (Reproduced with permission: Copyright 2020, AAAS)[24].

Meijie Chen is an Associate Professor in the School of Energy Science and Engineering at Central South University. He received his B.Eng., M.Eng., and Ph.D. degrees from School of Energy Science and Engineering at Harbin Institute of Technology in 2014, 2016 and 2019, respectively. He was a Visiting graduate student at Columbia University funded by CSC in 2018. His research interests are in the photothermal conversion, transport, storage and applications.

Dan Pang received her Bachelor degrees from Centre South University in 2020. She is now a master student at Centre South University. Her research interests include radiative cooling and nanoscale thermal management.

Xingyu Chen received her Master degrees from Centre South University in 2019. She is now a Ph.D. student at Centre South University. Her research interests include heat and mass transfer of nanofluids, solar thermal conversion and radiative cooling.

Hongjie Yan is a Professor in the School of Energy Science and Engineering at Central South University. He received his B.Eng. and Ph.D. degrees from School of Energy Science and Engineering at Central South University in 1999 and 2005. His research interests are multiphase fluid, computational fluid dynamics, and energy saving in industrial processes.

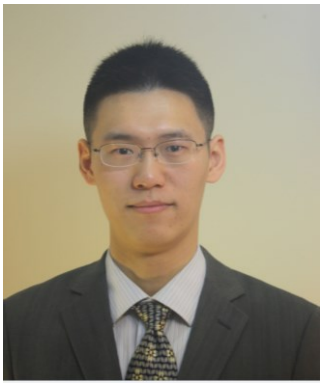

Yuan Yang is Associate Professor in the Department of Applied Physics and Applied Mathematics, Columbia University. He received his B.S. in physics from Peking University in 2007 and his Ph.D. in materials science and engineering from Stanford University in 2012. Then he worked as a postdoctoral researcher at MIT for 3 years. His research interests include electrochemical energy storage and conversion and thermal management.